LE3 B7
1949 A7
L35 S7
Cop. 1

A STUDY OF FATIGUE STRESSES IN MARINE PROPELLOR SHAFTING

by

WILLIAM CUMMING LEITH

A Thesis Submitted In Partial Fulfilment of

The Requirements For The Degree Of

MASTER OF APPLIED SCIENCE

In The Department

Of

MECHANICAL ENGINEERING

Thesis Supervisor:

Head of Department:

THE UNIVERSITY OF BRITISH COLUMBIA

October, 1949

A STUDY OF FATIGUE STRESSES IN MARINE PROPELLOR SHAFTING

ABSTRACT

This paper describes an investigation carried out to study the fatigue failures of a "keyed tapered-shaft assembly" as affected by the keyway. Two fatigue testing machines were built and used: one tested a keyed assembly in reversed bending, and the other tested a keyed assembly in reversed torsion or a combination of reversed bending and reversed torsion. Both sled-runner and round-ended keyways were tested and the failures were compared with a view to establishing a law of failure.

ACKNOWLEDGEMENT

The writer wishes to thank Professor W.O. Richmond for his guidance and advice during this investigation; Professor W. Opechowski for his help in obtaining recent papers on the atomic theory; The British Columbia Electric Railway Company Limited for the scholarship under which the research was conducted; and Mr. J.D. Leith for his assistance in constructing the two testing machines.

TABLE OF CONTENTS

LIST OF ILLUSTRATIONS

(Cont'd) LIST OF ILLUSTRATIONS

TABLES

A STUDY OF FATIGUE STRESSES IN MARINE PROPELLOR SHAFTING

The abnormal increase in the number of failures occurring in the tailshafts of E.C.2-S-C.1 Liberty Ships built during the recent war, has caused much concern in shipping circles. In 1947 "Liberty" Ships (1)[i] represented about 20 per cent of the world gross tonnage or 13½ per cent in number. Information at 1st December, 1948, revealed that altogether a total of 583 "Liberty" screwshafts have been renewed, including during the past three years about 100 casualties at sea with resulting loss of propellor. The cost of these breakdowns in salvage and demurrage charges alone needs no emphasis.

Most of the failures which have occurred near the large end of the tail shaft cone as shown in Fig. 1, seemed to be of two types; one due to corrosion fatigue and the other due to vibration stresses. Corrosion fatigue is usually indicated by a circumferential groove around the shaft at the end of the

i - See Bibliography

Fig. 1 A Typical Tailshaft Failure

bronze liner and is caused by a defective sealing ring. By 1947, failures from this cause had practically been eliminated.

When the propellor has been slack on the taper, a bronze deposit is usually found on the shaft indicating rubbing between the surfaces. Excessive bearing on the sides at the forward end of the keyway usually formed cracks at the root of the keyway.

Vibration stresses both torsional and bending, will increase beyond safe limits during excessive racing of the propellor. These stresses acting on the existing stress raisers can weaken the shaft by overstress and promote rapid failure by early cracking. Therefore, one can understand why fatigue cracks start at the forward corners of the keyway and on each side of the tapped hole for the forward key - retaining bolt.

Two fatigue testing machines were built with a view of studying the strength of keyed joints in shafts; one tested a keyed tapered-shaft assembly in reversed bending, and the other tested a keyed assembly in reversed torsion or a combination of reversed bending and reversed torsion. Tapered-shafts with sled-runner and round-ended keyways as shown in Fig. 2 were tested and a study was made of the types of fractures obtained by the different methods of stressing.

THEORIES OF STRENGTH

Since this paper describes an investigation of the fatigue failure of keyed connections, a theory of strength is given to provide the academic background.

For many years engineers and physicists have attempted to correlate the atomic bond strength and the yield strength of steel. As yet, no one has formulated a theory to explain it satisfactorily. However, X-ray diffraction is being used to study the effect of stress on the crystal structure. Most of the values of strength used today are based on the experimental results of tensile, bending, impact, and torsion tests.

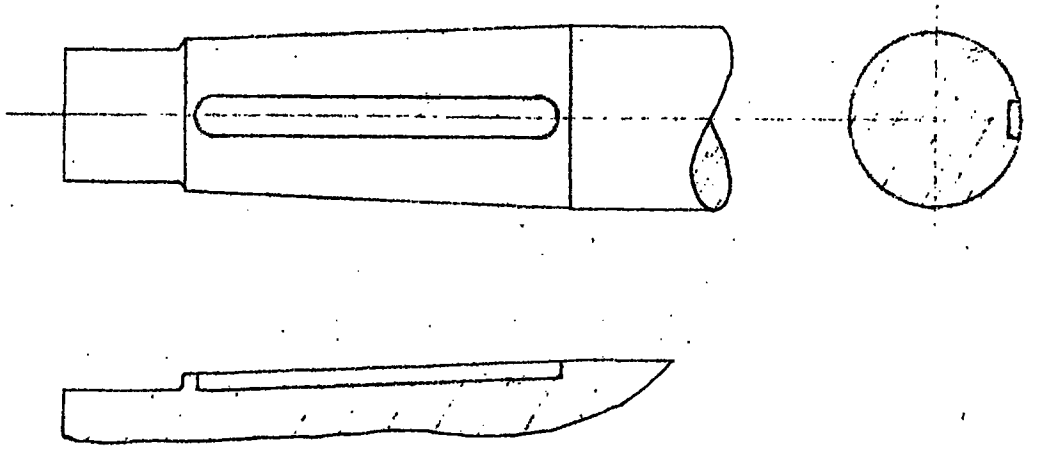

A) ROUND-ENDED KEYWAY

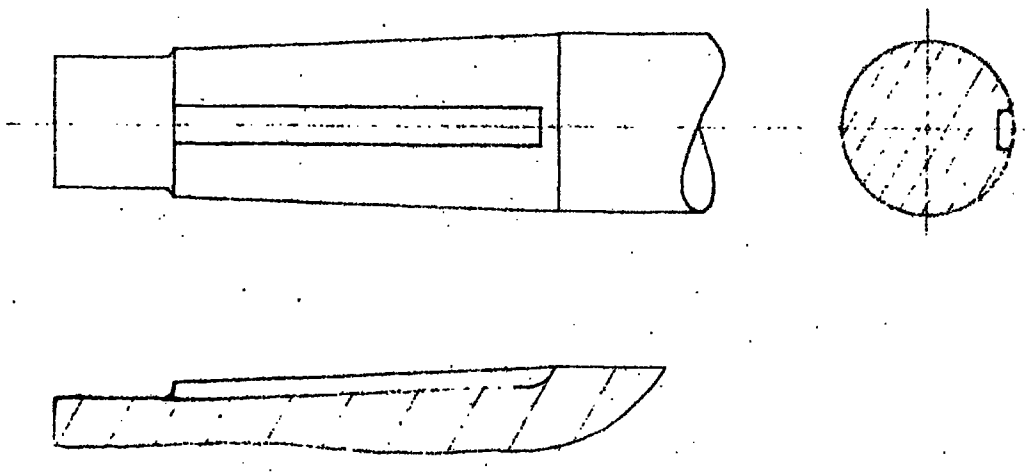

B) SLED-RUNNER KEYWAY

FIG. 2 TYPES OF KEYWAYS

ATOMIC THEORY OF STRENGTH

Although none of the present-day atomic theories explain fatigue in steel, the Dislocation Theory (2) does agree with experimental results for slip, work hardening, and yielding.

Elementary theoretical considerations, then, give us the following starting points for an atomic theory of strength (3).

(a) a perfect crystal with no dislocation, should be very strong; slip would not take place until a shear strain of several degrees had been applied.

(b) an otherwise perfect crystal containing a few dislocations would be very weak, since dislocations may be shown to move under the influence of a small shear stress.

The strength of metals, and the rate of flow and creep will be determined by two factors

(i) the rate at which dislocations are formed

(ii) the resistance to their motion

In discussing (i) it must be remembered that a dislocation is a long line of misfit, extending right through a crystal. If the cohesive forces binding two crystals together are nearly as great as those between planes of atoms in the body of the crystal, the strain energy along an edge of this type will be nearly as great as that of a dislocation, and little energy will be required to form a dislocation there and

to move it away. If this view is correct, crystal boundaries are the sources of dislocations; in single crystals, boundaries between elements of the mosaic must fulfil the same role. The condition for the formation of a dislocation is that cohesion across the crystal boundary shall give as much energy as cohesion within the crystal, and this will be the case only if all the atoms are in equivalent positions.

In discussing (ii), the factor preventing the motion of dislocations is the presence in the crystal of internal strains. Taylor suggested that the condition for the movement of a dislocation along a guide plane is that the relevant component of shear strain shall actually have the same sign at all points along the guide plane; if it does not, the dislocation will come to rest at a position of equilibrium.

Qualitatively, this theory leads to the conclusion that the yield strength of a metal is of the order of magnitude $G\delta_0$, where G is the elastic shear modulus and δ_0 is the mean internal strain.

A fatigue failure (4) involves three stages

(a) slip occurs and results in strain hardening and lattice distortions

(b) the fatigue crack starts

(c) the crack spreads along the path of least resistance, due to stress concentration. This proceeds until the cross section of the metal is reduced so much that the remaining portion breaks under the static load. Hence fatigue failures usually exhibit two zones; the brittle

zone due to the real fatigue action, and the fibrous zone having the same appearance as a failure under a static stress.

MAXIMUM SHEAR THEORY OF STRENGTH

Although we know that steel is not an ideal material, we apply the mathematical theory of elasticity (5) in general design. Its formulae are based on the following assumptions:

(a) steel is homogeneous or it can be divided infinitely into smaller particles without changing the strength stiffness properties.

(b) steel is isotropic or it has equal elastic stiffness in all directions.

(c) steel follows Hooke's law.

In the most general case, the stress conditions of a element of a stressed body is defined by the magnitude of the three principal stresses σ_X , σ_Y , σ_Z as shown in Fig. 3. The algebraic values of the principal stresses is assumed to have the following relation, in which the tension is taken positive and compression negative.

$$\sigma_x > \sigma_Y > \sigma_z$$

The maximum shear theory states that yielding begins when the maximum shearing stress becomes equal to the maximum shearing stress at the yield point in simple tension. Since the maximum shearing stress is equal to half the difference between the maximum and the minimum principal stress, the

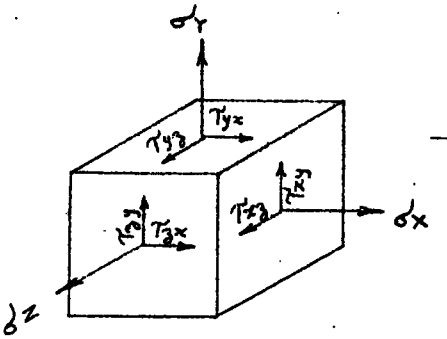

FIG. 3 NORMAL AND SHEAR STRESSES

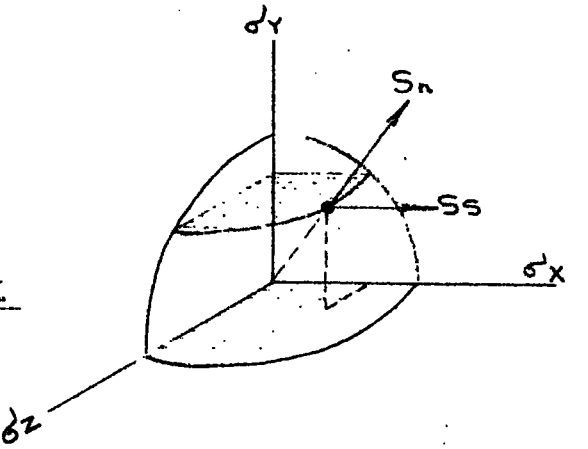

FIG. 4 MOHR'S SPHERE

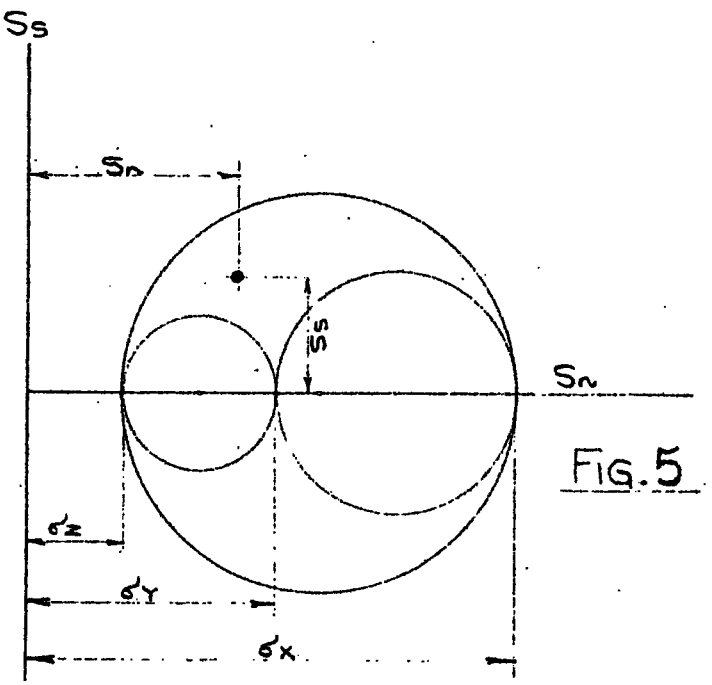

FIG. 5 MOHR'S STRESS PLANE

condition for yielding is $\frac{1}{2}(\sigma_x - \sigma_y) = \frac{1}{2}\sigma_{Y.P.}$

The shearing stress (6) on a cross-section parallel to the yz plane may be divided into two components τ_{xy} and τ_{xz}, parallel respectively to the y and z axes. In this method of designation of stress components, the single subscript of a normal stress such as σ_x and the first subscript of a shearing stress such as τ_{xy} correspond with the direction of the normal to the section, while the second subscript of τ_{xy} indicates the direction in which the component is to be taken.

The values of the principal shearing stresses are defined as the radii of Mohr's three principal circles shown in Fig. 4 and 5. For the general state of stress, the maximum shearing stress occurs at sections making angles of 45 degrees with the sections across which the principal stresses act.

Timoshenko (5) describes a simple procedure to estimate the fatigue strength for different combinations of variable and steady loads. This method is based on:

(a) the maximum shear theory for ductile materials

(b) the yield stress for steady stresses

(c) the endurance limit for variable stresses

(d) stress concentration in ductile materials is important for variable loads only.

(e) the assumed law of failure for combined steady and variable stresses is shown in Fig. 6 and is conservative compared to Gough's experimental results.

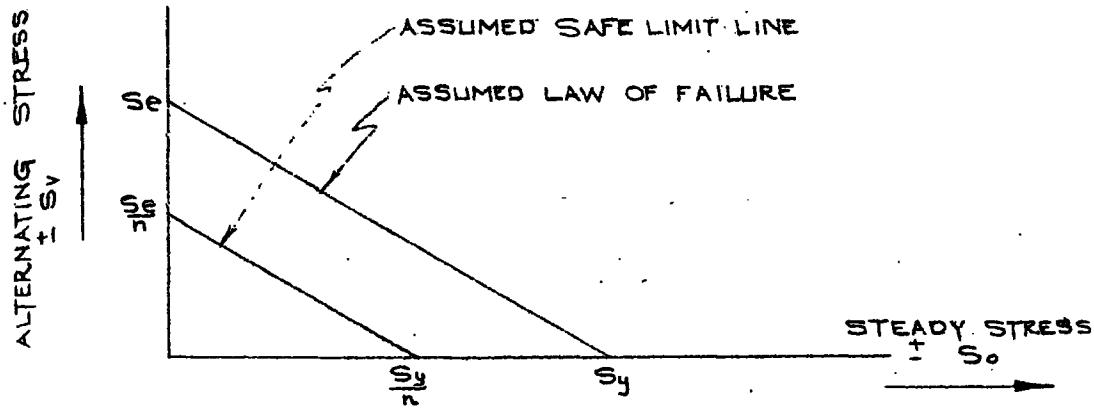

FIG. 6 A LAW OF FAILURE.

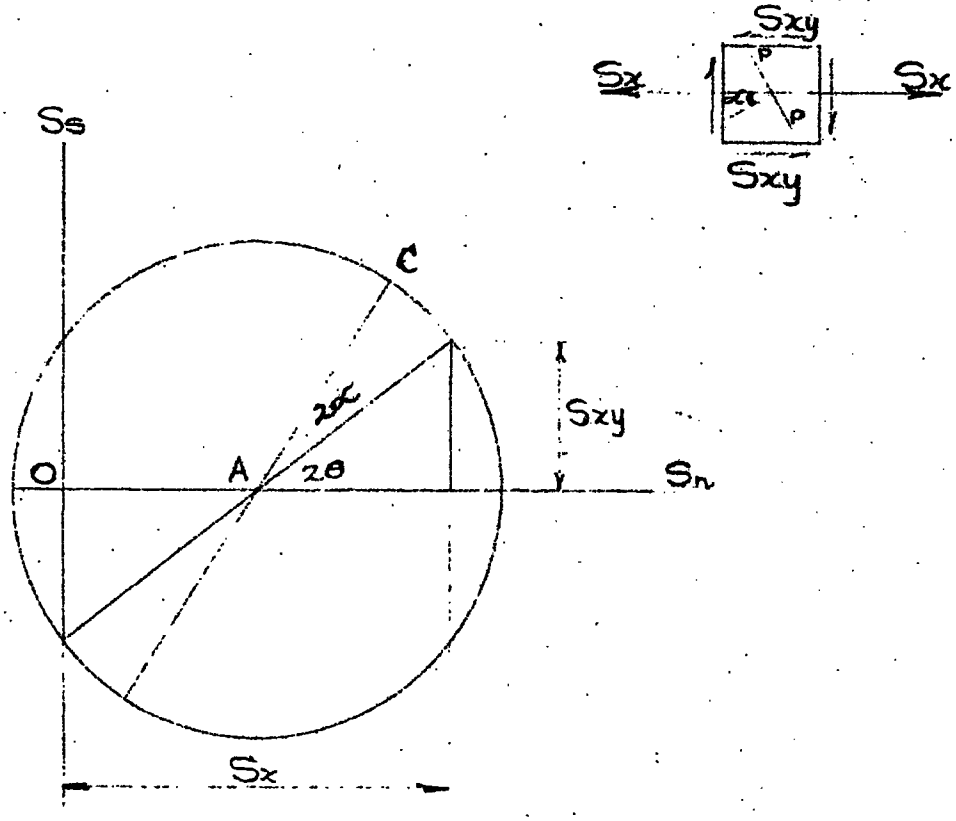

FIG. 7 COMBINED STRESS PLANES

Se = endurance limit for reversed stress

(failure condition for complete load reversal)

Sy = yield point stress in tension

n = factor of safety

The equation of the failure line in terms of the steady stress So and the cyclic stress Sv is:

$$\frac{So}{Sy} + \frac{Sv}{Se} = 1$$

If we introduce n, the equation of the safe limit line is:

$$\frac{So}{Sy} + \frac{Sv}{Se} = \frac{1}{n}$$

Applying these assumptions to shaft design, we shall consider some important cases.

Case 1 a steady torque To and a cyclic torque Tv

loading = $To \pm Tv \sin wt$

shear stress due to To

$$(Ss)o = \frac{To\ d}{2J} = \frac{16\ To}{\pi d^3}$$

shear stress due to Tv

$$(Ss)v = \frac{kTv\ d}{2J} = \frac{k16\ Tv}{\pi d^3}$$

k = stress concentration factor due to a fillet, keyway, etc.

Since

$$\frac{(Ss)o}{(Ss)y} + \frac{(Ss)v}{(Ss)e} = \frac{1}{n}$$

$$\frac{16To}{\pi d^3\ (Ss)y} + \frac{K16Tv}{\pi d^3\ (Ss)e} = \frac{1}{n}$$

$$(Ss)y = \frac{Sy}{2} \qquad (Ss)e = \frac{Se}{2}$$

Hence $$d = \sqrt[3]{\frac{32n}{\pi}\left(\frac{To}{Sy} + \frac{kTv}{Se}\right)}$$

Case 11 a steady moment Mo and a cyclic moment Mv

loading = $Mo \pm Mv \sin wt$

normal stress due to Mo $$So = \frac{Mod}{2I} = \frac{32\ Mo}{\pi d^3}$$

normal stress due to Mv $$Sv = \frac{kMv\ d}{2I} = \frac{k32Mv}{\pi d^3}$$

Since $$\frac{So}{Sy} + \frac{Sv}{Se} = \frac{1}{n}$$

$$\frac{32\ Mo}{\pi d^3\ Sy} + \frac{k32\ Mv}{\pi d^3\ Se} = \frac{1}{n}$$

Hence $$d = \sqrt[3]{\frac{32n}{\pi}\left(\frac{Mo}{Sy} + \frac{kMv}{Se}\right)}$$

Case 111 a steady torque To, a steady moment Mo, a cyclic torque Tv, and a cyclic moment Mv

loading = $(Mo \pm Mv \sin wt) + (To \pm Tv \sin wt)$

In this case we have combined normal and shear stresses which are shown in Fig. 7 for a given plane P. P.

normal stress due to $Mo \pm Mv$ $\quad Sx = \frac{Mo\ d}{2I} \pm \frac{kMv\ d}{2I}$

shear stress due to $To \pm Tv$ $\quad Sxy = \frac{To\ d}{2J} \pm \frac{kTv\ d}{2J}$

Ss = combined shear stress on plane P. P.

$= AC \sin 2(\theta + A)$

$= \frac{Sx}{2} \sin 2A + Sxy \cos 2A$

Hence $\quad Ss = \left(\frac{Mo\ d}{4I} + \frac{kMv\ d}{4I}\right) \sin 2A + \left(\frac{Tod}{2J} + \frac{kTvd}{2J}\right) \cos 2A$

$$(Ss)o = \frac{Mo\ d}{4I} \sin 2A + \frac{To\ d}{2J} \cos 2A$$

$$(Ss)v = \frac{kMv\ d}{4I} \sin 2A + \frac{k\ Tv\ d}{2J} \cos 2A$$

Substituting

$$\frac{1}{n} = \frac{(Ss)o}{(Ss)y} + \frac{(Ss)v}{(Ss)e}$$

$$\frac{1}{n} = \frac{\left(\frac{Mod}{4I} \sin 2A \quad \frac{Tod}{2J} \cos 2A\right)}{(Ss)y} + \frac{\left(\frac{kMvd}{4I} \sin 2A \quad \frac{kTvd}{2J} \cos 2A\right)}{(Ss)e}$$

Hence

$$d = \sqrt[3]{\frac{32n}{\pi}\left(\frac{Mo \sin 2A + To \cos 2A}{Sy} + \frac{kMv \sin 2A + kTv \cos 2A}{Se}\right)}$$

where

$$(Ss)y = \frac{Sy}{2}, \quad (Ss)e = \frac{Se}{2}; \qquad \tan 2A = 1/2\ \frac{(Mo + k\ Mv)}{(To + k\ Tv)}$$

ANAYLSIS OF A KEYED PROPELLOR ASSEMBLY

The fatigue strength of a keyed propellor assembly as shown in Fig. 8 can be estimated by combining the torsional, bending and thrust stresses for ideal conditions of loading, that is, calm seas and a fully submerged propellor. But there are a number of indeterminate stresses which may occur individually or together; the maximum torsional vibration stresses when the propellor is racing, the maximum bending stresses when the ship is in ballast, and the clamping stresses at the top of the taper by the edge of the propellor boss recess and by the edge of the shaft liner.

A complete theoretical solution for the stress concentration at a keyway does not exist, but the "hydrodynamical analogy" (5) is useful for discussing the torsion of shafts. The twisting of shafts of uniform cross-section is mathematically identical to the motion of a frictionless fluid moving with uniform angular velocity inside a shell having the same section as the bar. The velocity of the circulating fluid at any point is taken as representing the shearing stress at that point of the cross section of the bar when twisted.

For the case of a keyway with sharp corners (See Fig.9) this analogy indicates a zero velocity of the circulating fluid at the outside corners (points M-M); hence the shearing stress in the corresponding torsion problem is zero at such points. Similarily, this analogy indicates an infinite velocity at the inside corners (points N-N), the vertices of

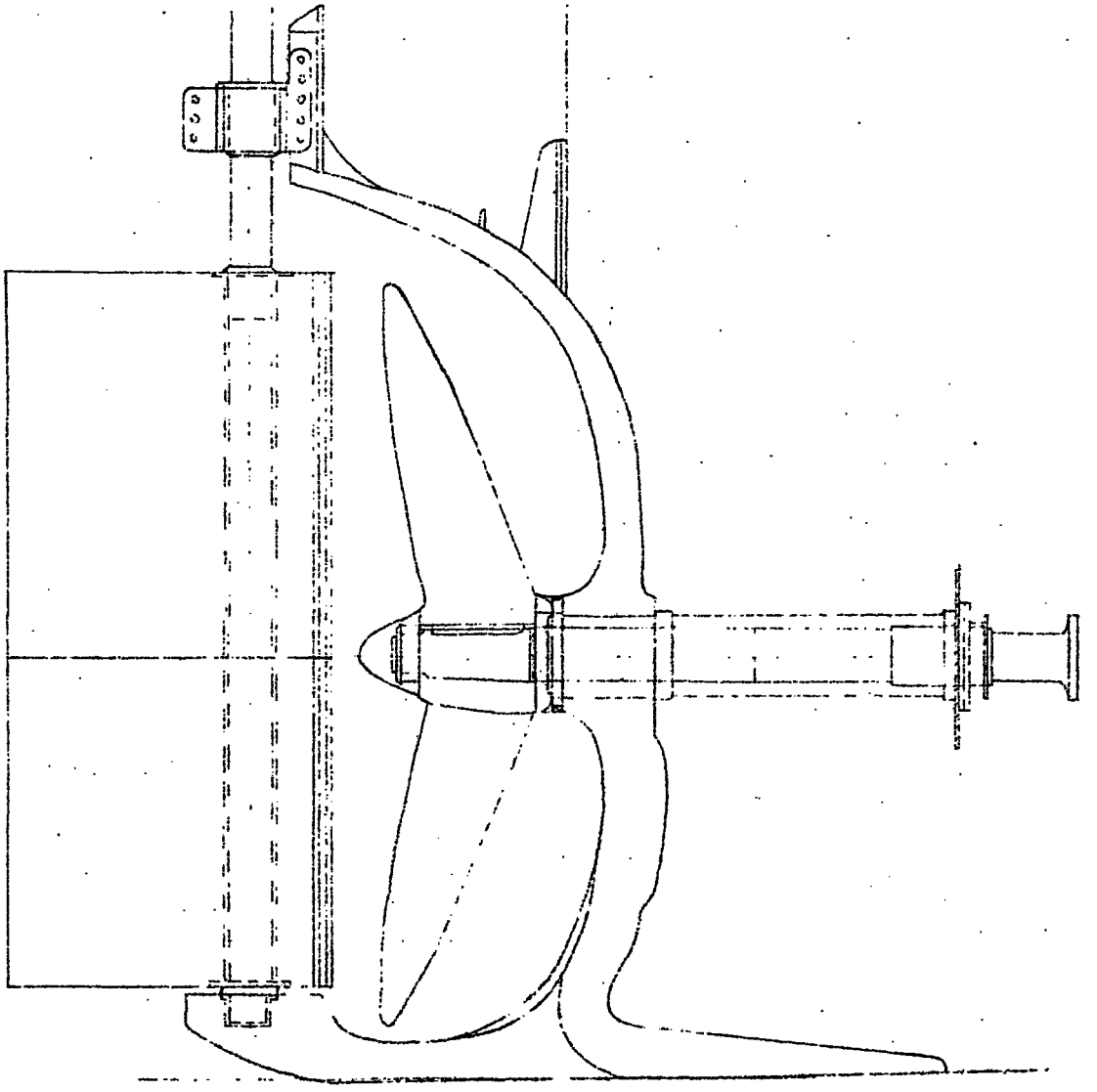

FIG. 8 KEYED PROPELLOR ASSEMBLY OF A "LIBERTY" SHIP

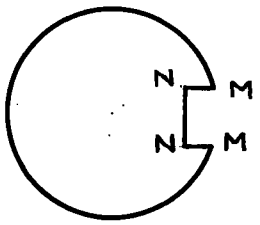

Fig. 9 Hydrodynamical Analogy

the reentrant corners; hence the shearing stress is also infinite at such points. Since a keyway with absolutely sharp corners cannot be cut, the reentrant corners will have a small radius of fillet and a finite stress distribution. A stress concentration factor "K" is used to denote the ratio of the maximum stress to the nominal stress; that is, $K = \frac{\sigma_{max.}}{\sigma_{nom.}}$. Figs. 10 and 11 show published values of the stress concentration factor "K" as have been obtained by the soap film method and the photoelastic method of measuring stress.

Several experimenters have carried out endurance tests to determine the nominal stress concentration factors for sled-runner and round-ended keyways, but because of size effect and clamping stress S. Archer (1) maintains that until large-scale tests of full-size propellors are made, there seems to be little to choose between the two types of keyways.

Under steady conditions in smooth water, with some bending fatigue present, such as when the propellor is partly submerged in the ballasted conditions, it is estimated from the evidence (1) so far available that the fatigue strength of a well fitted propellor assembly, expressed in terms of nominal reversed torsional stress, may be of the order of 6000 psi. It should always be borne in mind, however, that this estimated value may be seriously reduced in service on account of a variety of causes, such as extremes of stress concentration

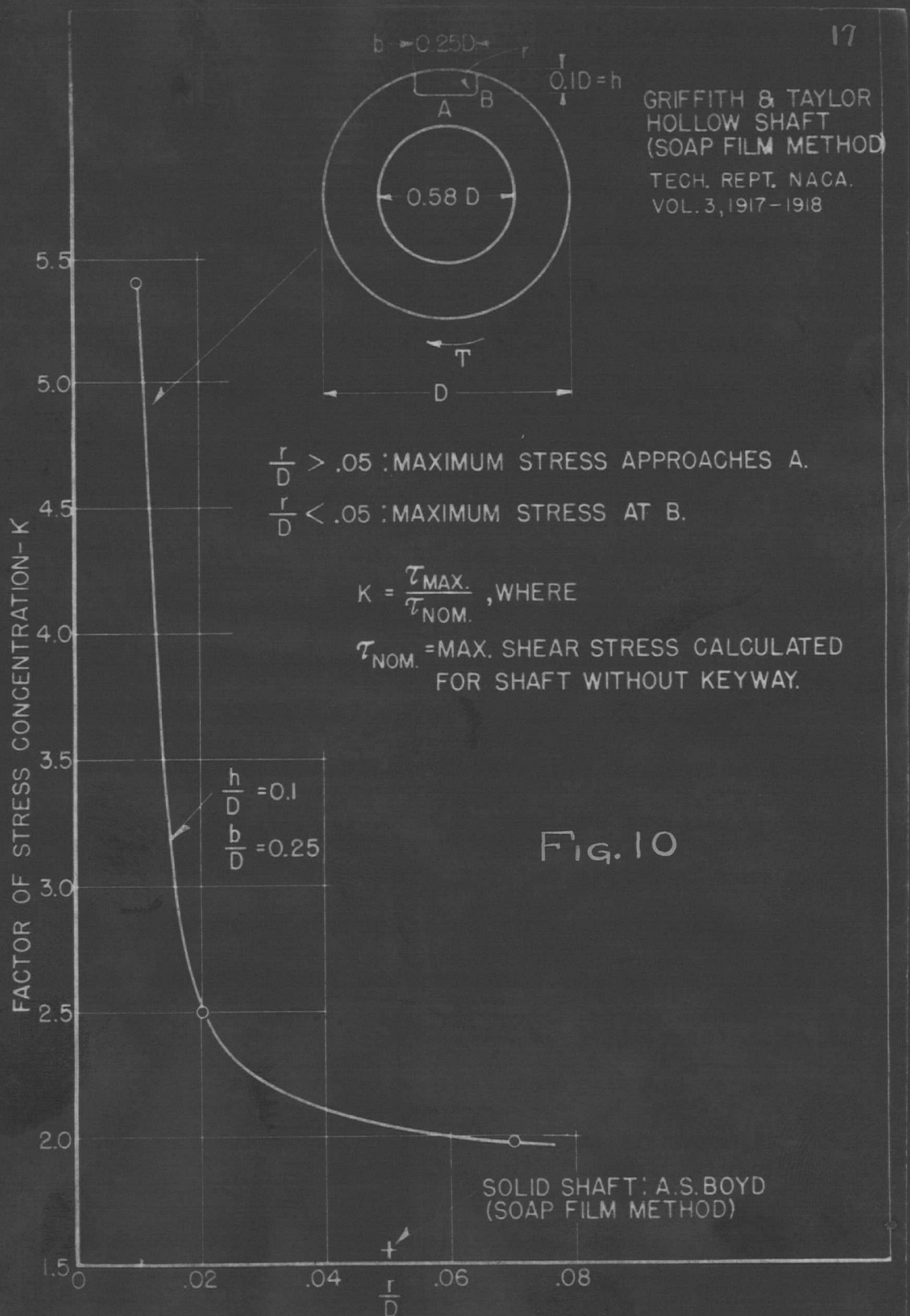

Fig. 10

M LEVEN
7-2-47

WESTINGHOUSE
RESEARCH LABORATORIES

CURVE 304511-D

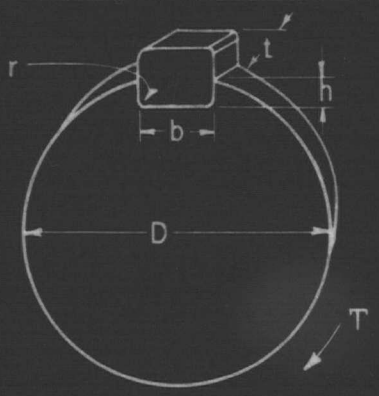

GIBSON & GILET – 100% TORQUE TRANSMITTED BY KEY. $\frac{h}{D} = 0.081$; $\frac{b}{D} = 0.25$

(PHOTOELASTIC: 2 DIMENSIONAL)

JOURNAL INST. OF ENGINEERS, AUSTRALIA
VOL. 10, NOS. 11 AND 12, NOV., DEC., 1938

$$K = \frac{\tau_{MAX.}\ (PHOTOELASTIC)}{\tau_{NOM.}},$$

WHERE $\tau_{NOM.} = \frac{16\,T}{tD^3}$

Fig. 11

GIBSON & GILET – APPROX. 50% TORQUE TRANSMITTED BY KEY.

SOLAKIAN & KARELITZ
$\frac{h}{D} = 0.125$; $\frac{b}{D} = 0.25$

FACTOR OF STRESS CONCENTRATION – K

10
9
8
7
6
5
4
3
2
1

0 .02 .04 .06 .08

$\frac{r}{D}$

M. LEVEN

WESTINGHOUSE RESEARCH LABORATORIES

CURVE 304510-D

arising from machining erros, badly fitted parts, corrosive envirnment, and previous overstress.

Stress concentration at a keyway (7) is best realized with the aid of photoelasticity (8) which utilizes the optical effect of stresses on a transparent model. Certain transparent materials (9) when stressed become birefringent, that is if a beam of light be passed through the stressed material it is split up into two plane polarized waves of light which vibrate in planes at right angles to each other. At each point in the material the two planes coincide with the directions of the principal stresses, and the birefringence persists only while the material is stressed. The waves are each retarded in passing through the material, the amount of retardation depending on the corresponding principal stresses and on the thickness of the material. Thus, on emergence, the two waves are retarded relative to one another, or out of phase, by an amount proportional to the difference of the principal stresses. To observe the relative retardation it is necessary to resolve the two component waves in one direction. This may conveniently be done by using an analysing unit in the emergent beam of light. Due to the phase difference between the two components an interference phenomenon will then be produced, and at each point where the phase difference is half a wave length, there will be complete extinction. Such points cause dark bands which will be visible in the form of fringes on a suitable screen. Therefore by using a two dimensional model, the resulting fringe pattern is an indication of the principal stress

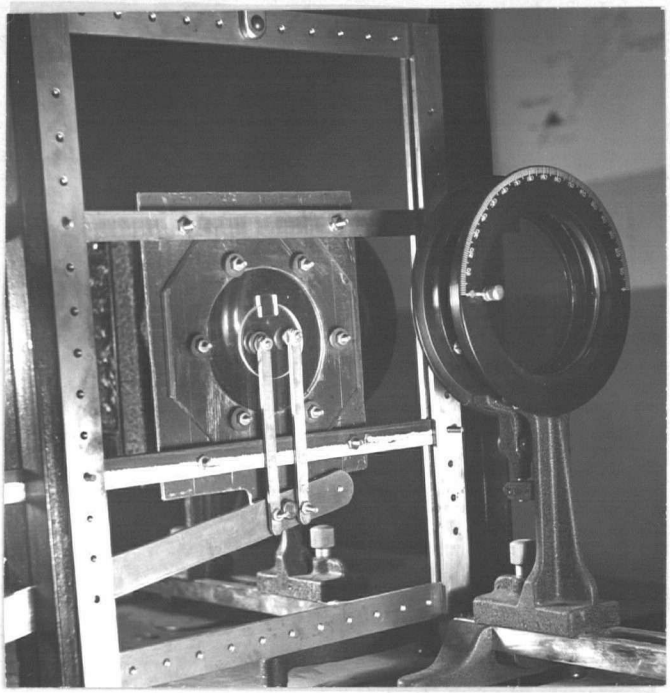

12

Fig. 12 Keyed Shaft Assembly Model

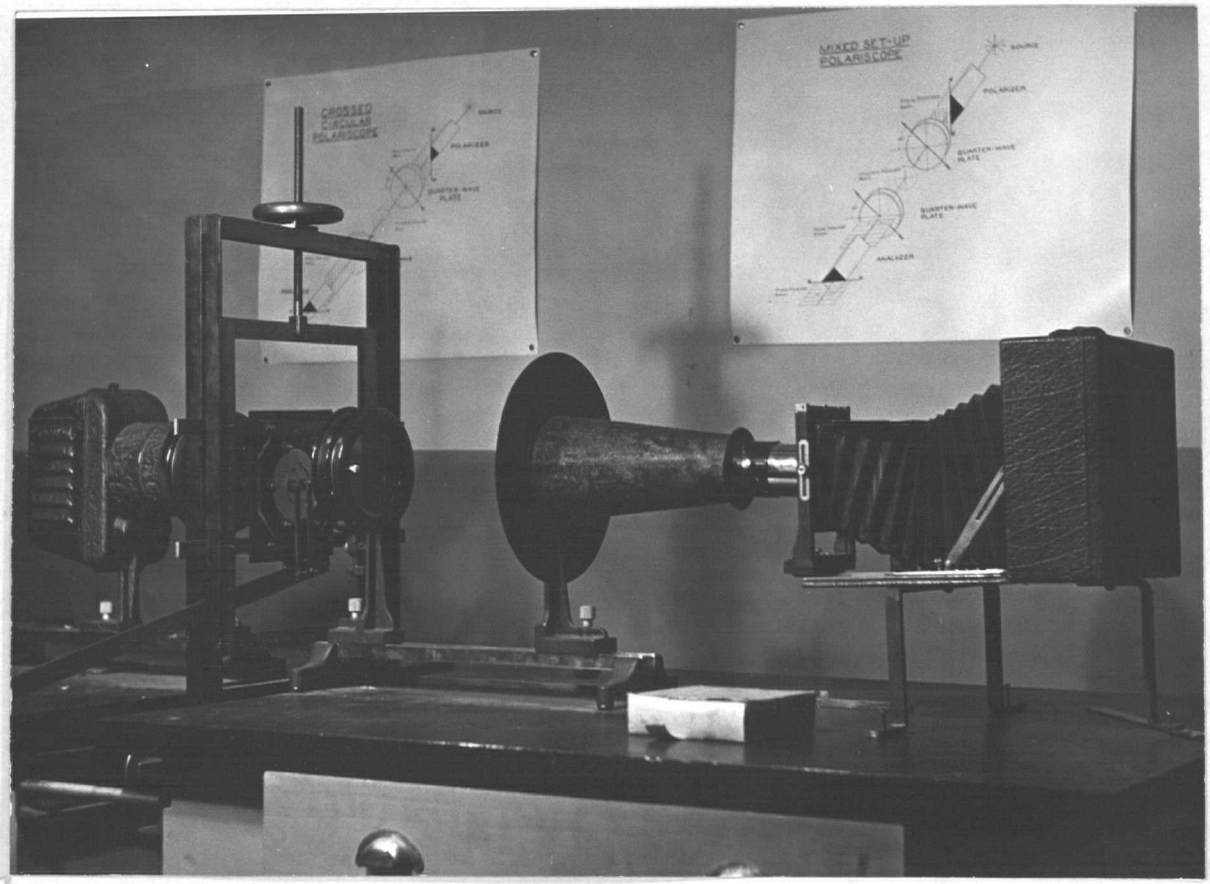

13

Fig. 13 Photoelastic Apparatus at U.B.C.

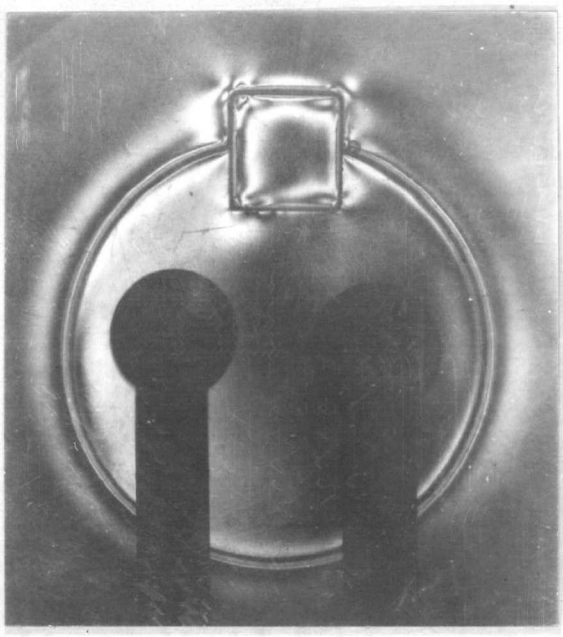

No Load

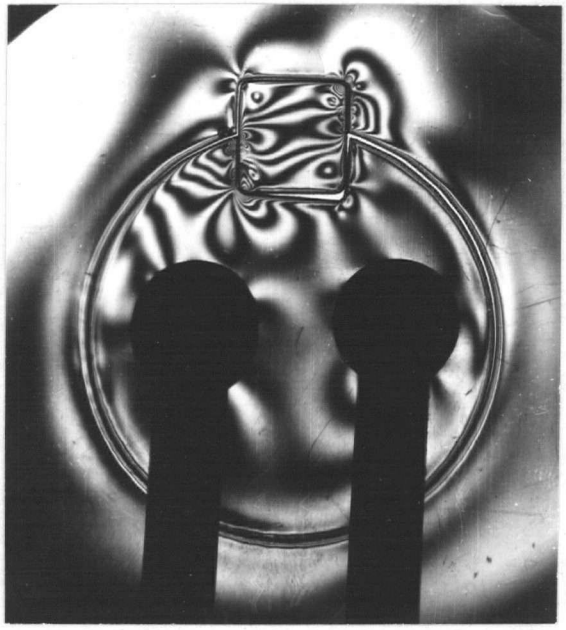

Load - 2 lbs.

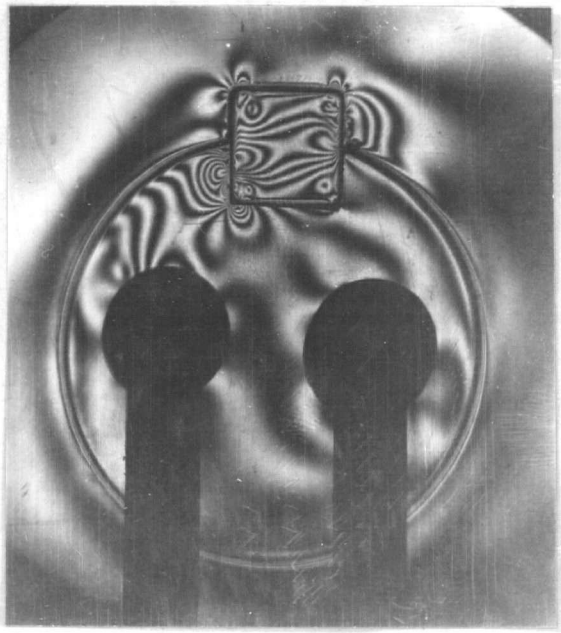

Load - 4 lbs.

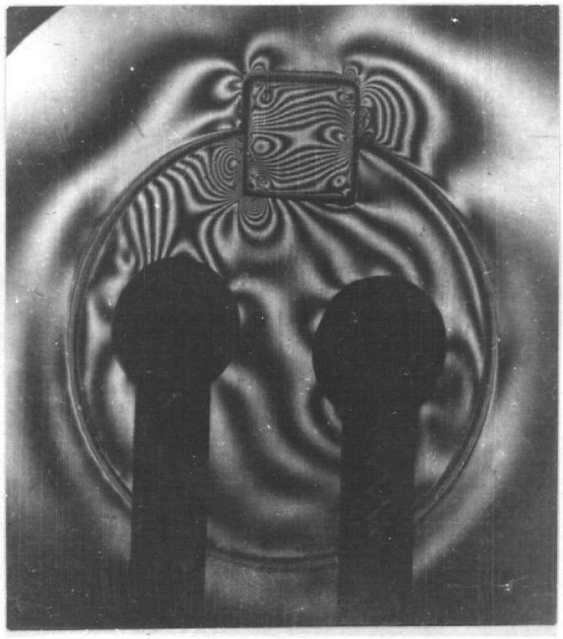

Load - 5 lbs.

Fig. 14 Stress Patterns in a Keyed Shaft assembly

difference at all points in the model. By suitable calibration the stress difference per fringe can be determined.

The writer made the keyed shaft assembly shown in Fig. 12 and studied it in the photoelastic apparatus of the Mechanical Department shown in Fig. 13. The stress concentrations at the reentrant corners are especially obvious in Fig.14 and demonstrate the detrimental effect of keyways.

Some revisions in the keyway design of "Liberty" tailshafts have been made to increase their fatigue strength. The original keyway as shown in Fig. 15, a tracing of the Burrard Dry Dock specifications of 1943, was of the round-ended type with no regulations governing the fillet. In 1947, Mr. W. O. Richmond (13) recommended a sled-runner keyway with a rounded fillet (this was later adopted) and shot-peening of the forward end of the keyway.

The revised keyway as shown in Fig. 16, a tracing of the Baldwin Locomotive Works specifications approved by the American Bureau of Shipping in 1948, is of the sled-runner type with a 3/16 in. fillet and has its edge broken with a file. The key has a 1/4 in. chamfer on all sides and is to be held in place by two jack-screws. In addition, the key has 1/8 in. saw cuts at the forward corners to transfer the load more equally throughout its length. Furthermore, tailshafts are to be drawn and inspected every two years rather than three.

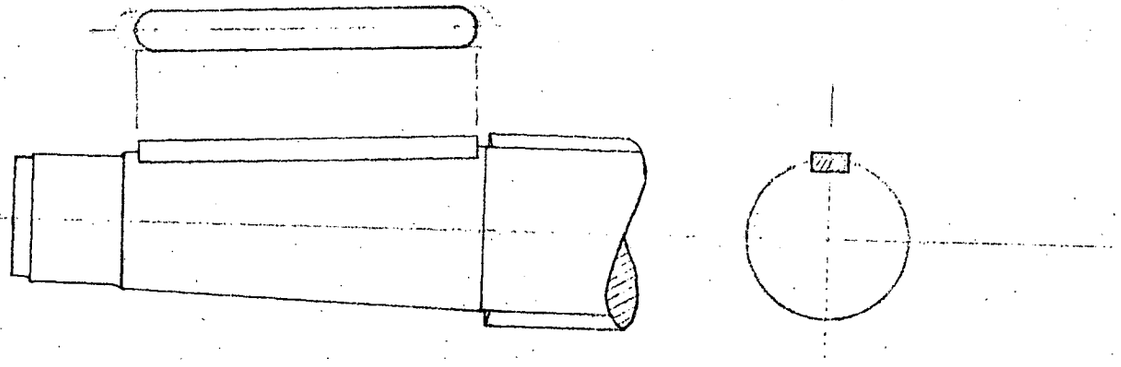

FIG. 15 ORIGINAL KEYWAY

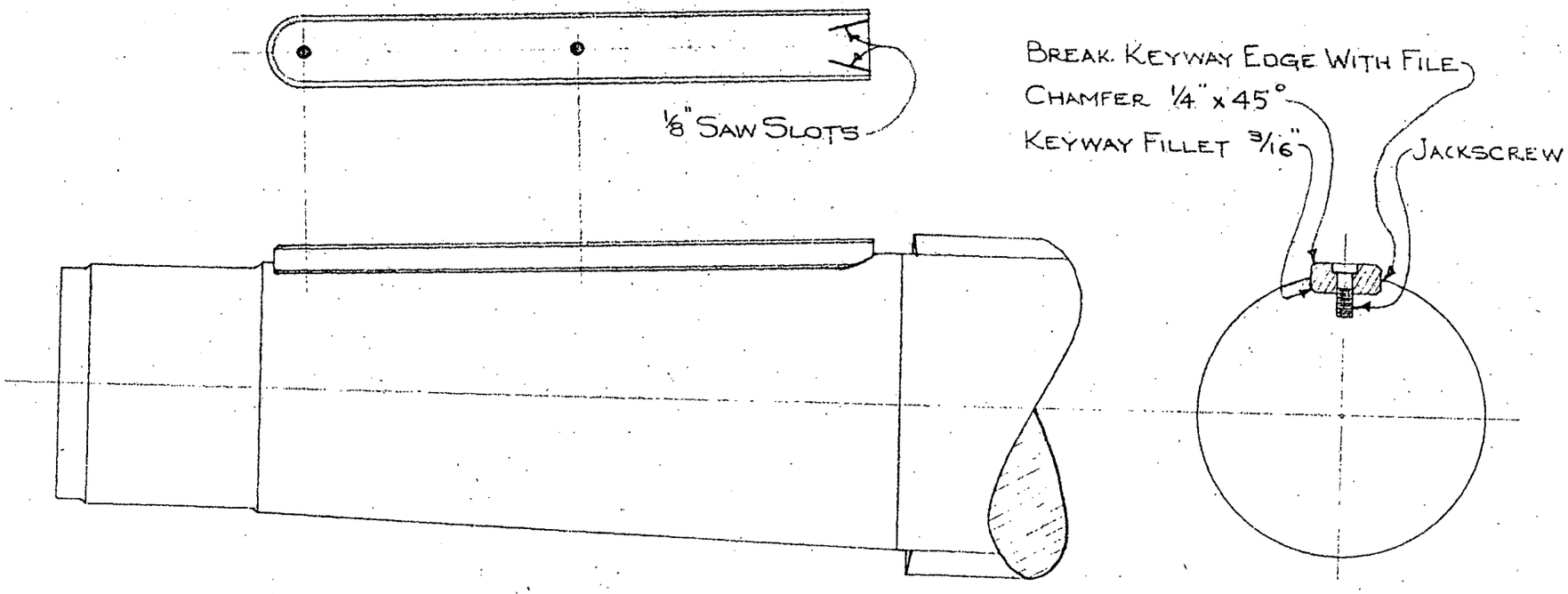

FIG. 16 MODIFIED "LIBERTY" KEYWAY

FATIGUE TESTING MACHINES

Economy and machining difficulties limited the test bar to a 3/4 in. diameter shaft with a 3/16 in. keyway. Using this shaft size as a basis in the design, the two testing machines were built to subject keyed tapered-shafts to repeated reversed stresses. In all tests, a known load was applied and the number of stress cycles was measured with a counter. Since these machines were constructed as preliminary models, a list of suggested improvements is given in the Recommendations.

The writer wishes to acknowledge that both machines were suggested by current literature: the bending machine is similar to one developed at the University of Illinois (10), and the eccentric of the torsion machine resembles one designed by Holley (11).

REVERSED BENDING MACHINE

The reversed bending machine is essentially a piece of steel tubing mounted between two ball bearings. One end is driven by a motor and the other end contains a tough steel bushing which supports the test shaft. The rotating test bar mounted as a cantilever beam, is loaded transversely with a known weight as shown in Figs. 17 and 18. Fig. 19 shows the details of the machine.

The large end of the tapered cone, which is the critical section in loading, has shearing stresses as well as

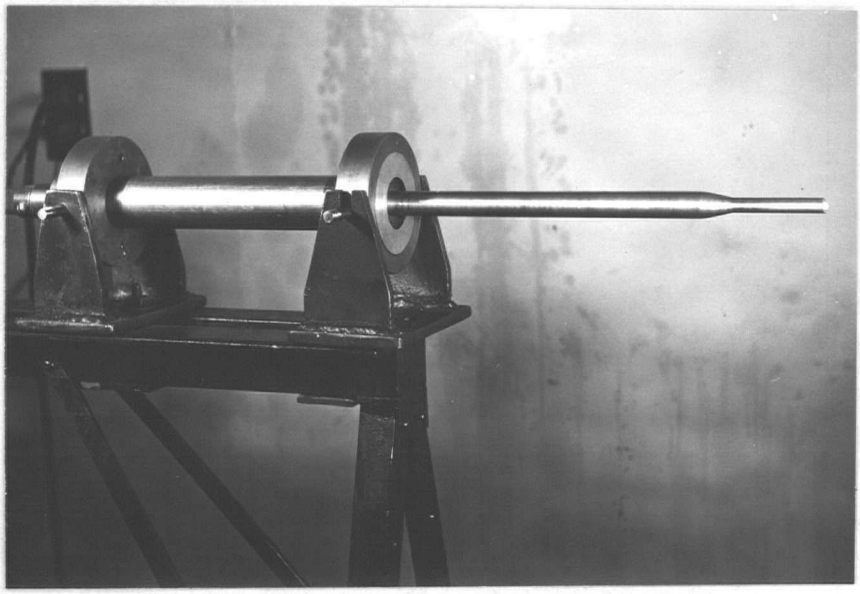

Fig. 17 Reversed Bending Machine

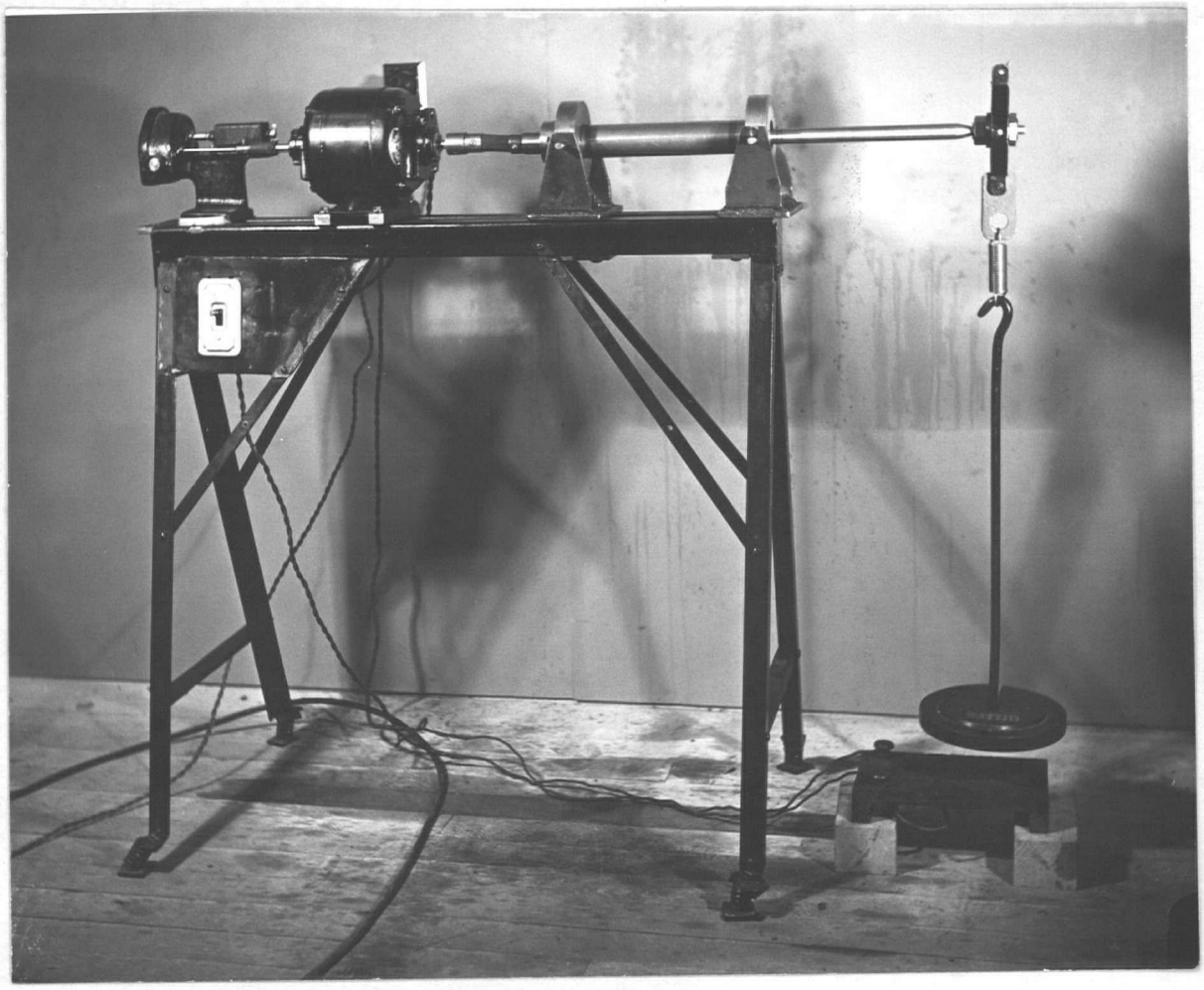

Fig. 18 Reversed Bending Machine - General Arrangement

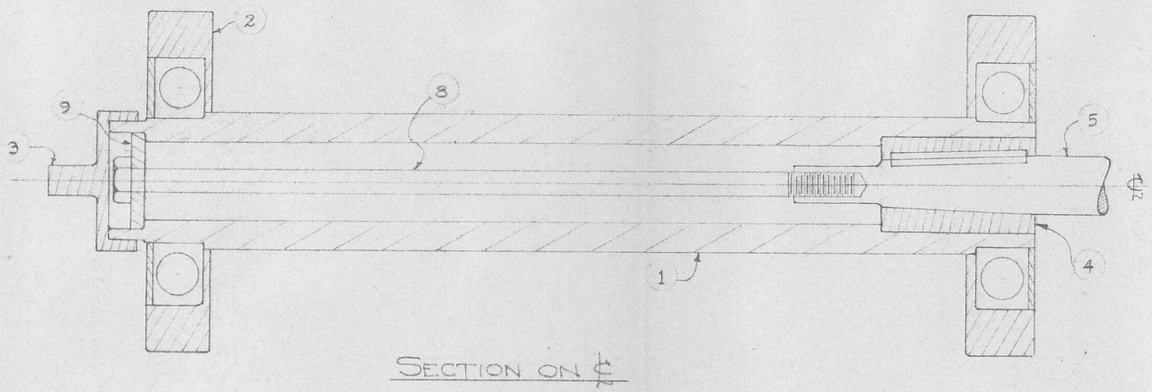

SECTION ON ℄

BILL OF MATERIAL.

No.	PART	QUAN.	REFERENCE
1	TUBE	1	MK "A"
2	BEARING CASES	2	"B"
3	COUPLING	1	"C"
4	COLLAR	1	"D"
5	TEST BAR		"E"
6	BRACKET	1	"F"
7	BRACKET	1	"G"
8	BOLT	1	"H"
9	WASHER	1	"I"
10			

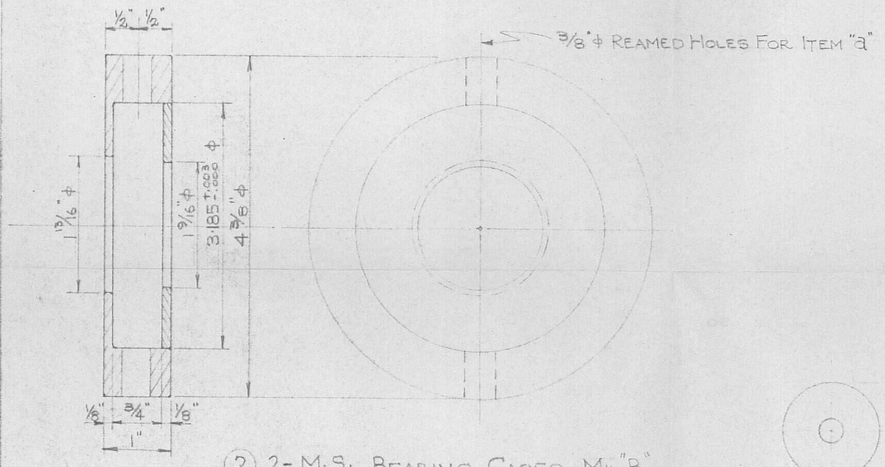

② 2-M·S· BEARING CASES MK "B"

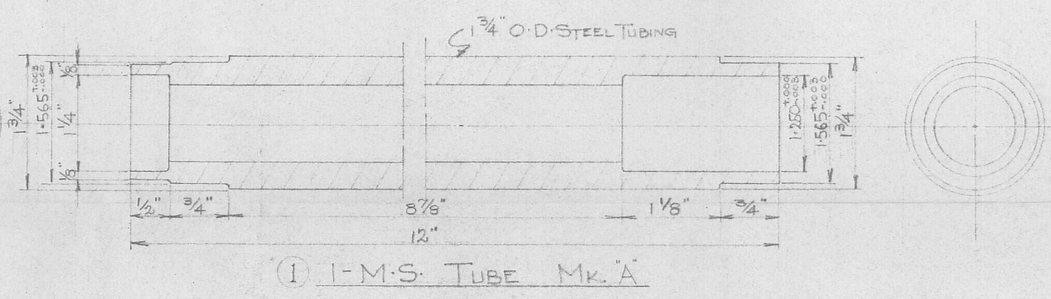

① 1-M·S· TUBE MK "A"

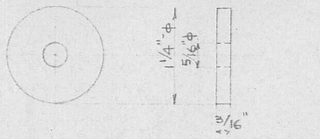

⑨ 1-M·S· WASHER MK "I"

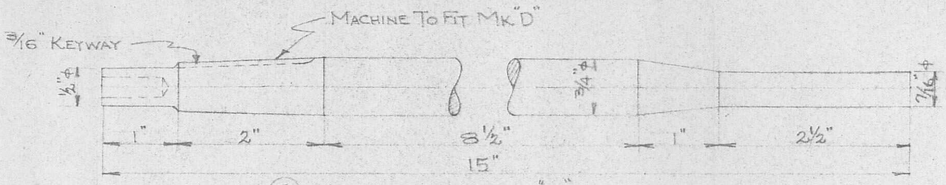

⑤ 1-TEST BAR MK "E"

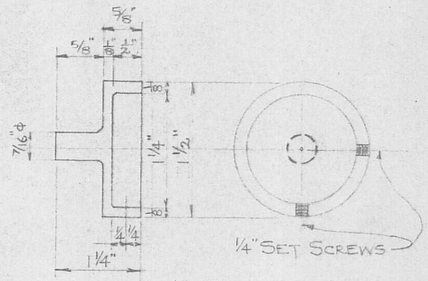

③ 1-M·S· COUPLING MK "C"

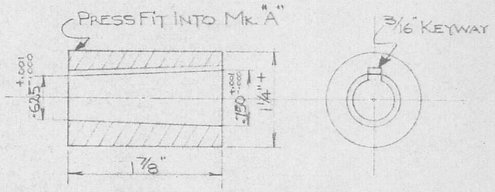

④ 1-S·T·S· COLLAR MK "D"

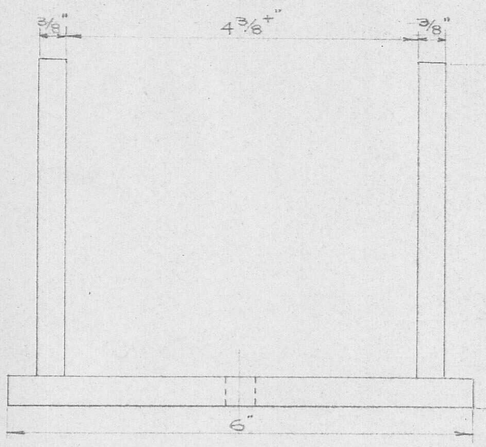

⑥ 1-M·S· BRACKET MK "F"

⑦ 1-M·S· BRACKET MK "G"

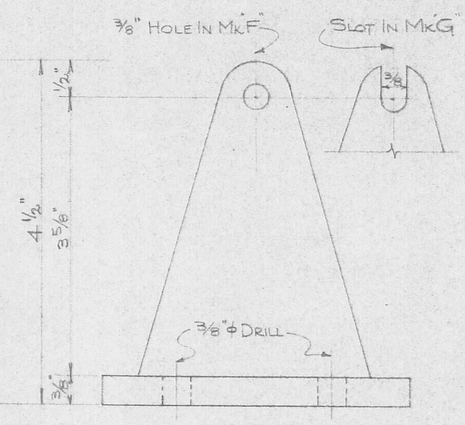

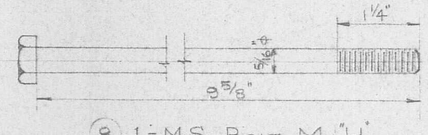

⑧ 1-M·S· BOLT MK "H"

MECHANICAL ENGINEERING
UNIVERSITY OF BRITISH COLUMBIA

REVERSED BENDING MACHINE

SCALE 9" = 1'-0"	MAY 1949
DRAWN BY Wm C. Leith	DRAWING NO. FIG. 19

the maximum bending stresses acting on it. However, the stress concentration at the forward end of the keyway usually causes failure there. The nominal stresses were calculated for each specimen and are listed in Table I.

As the machine ran smoothly for all tests, no modifications were necessary.

REVERSED TORSION MACHINE

The reversed torsion machine consists mainly of the torsion arm which twists one end of the test bar, while the other end is held firmly in the torsion block. A link connects the arm to the eccentric plate. By adjusting the slotted eccentric plate, the angular displacement of the arm and hence the applied torque, can be varied. The eccentric is mounted on a shaft directly connected to a 3/4 hp Baldor variable-speed motor; for details of this motor refer to (12). Fig. 20 shows the general arrangement of the machine and Fig. 21 shows a view of the eccentric. The details of the machine are given in Fig. 22.

The machine was fastened to the concrete floor with anchor-bolts to overcome the vibration caused by the unbalance of the eccentric. Also, the running speed was reduced from 1800 to 1000 rpm to lessen wear at the link-eccentric connection. However, a little movement which was noticed in the torsion block was assumed due to flexibility in the machine itself.

TABLE 1 REVERSED BENDING DATA

Number	Keyway	Bending Stress	Shear Stress	Number of Cycles	Remarks
1	SR	13600	113	22624000	UNBR
		21700	171	507000	BR
2	SR	16300	128	5012000	BR
3	SR	14000	131	100417000	UNBR
		16800	156	2204000	BR
4	RE	16200	128	1044000	BR
5	RE	13600	128	3430000	BR
6	RE	10800	85	30577000	UNBR
		13600	106	3818000	BR

SR = sled-runner keyway

RE = round-ended keyway

BR = broken

UNBR = unbroken

$$\text{Bending Stress} = \frac{Mc}{I}$$

$$\text{Shear Stress} = \frac{P}{A}$$

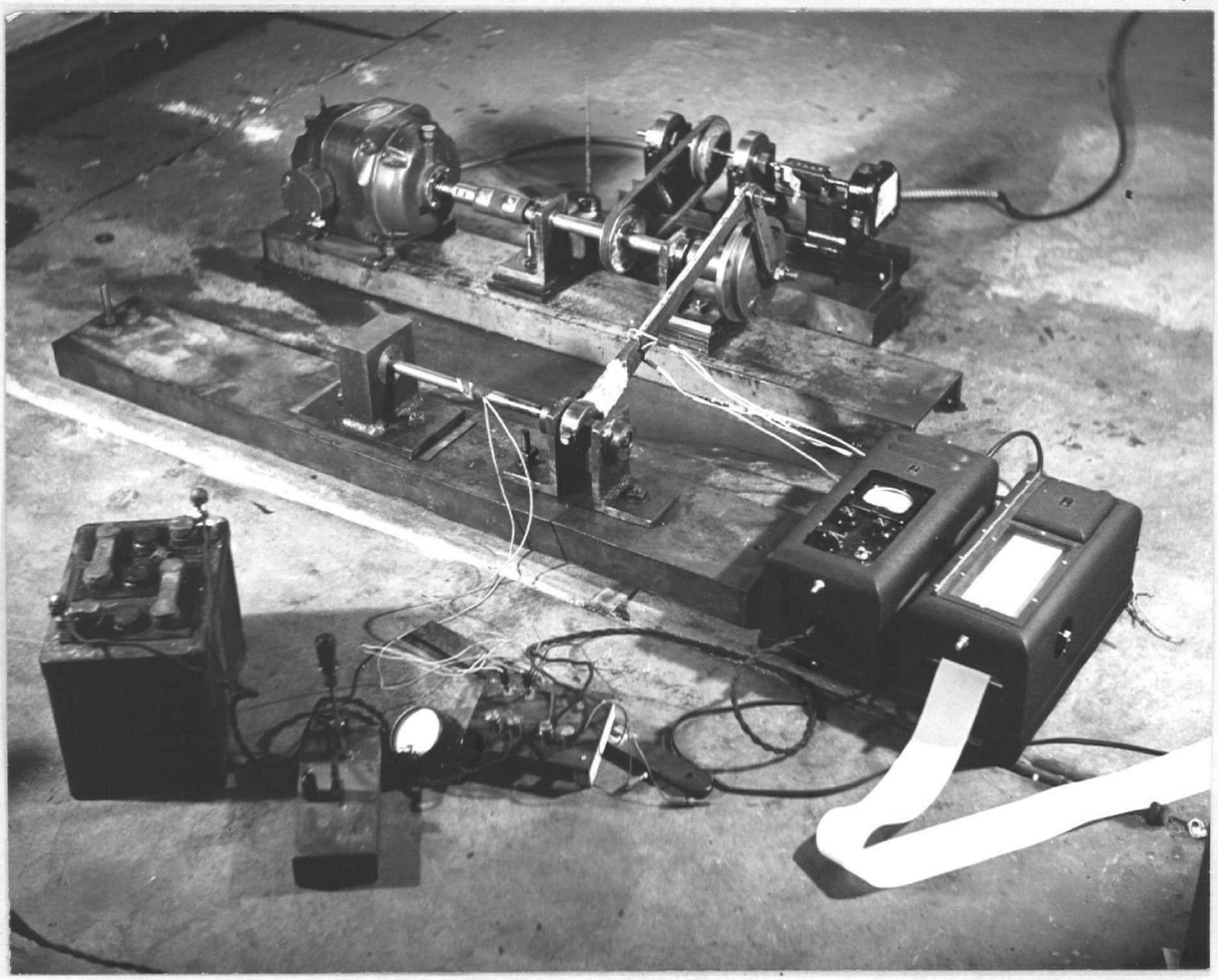

Fig. 20 Reversed Torsion Machine - General Arrangement

Fig. 21 Torsion Arm and Eccentric

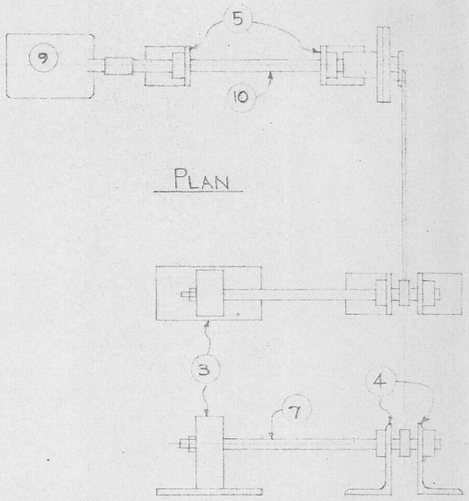

PLAN

ELEVATION

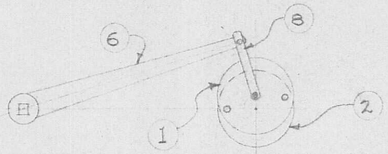

END VIEW

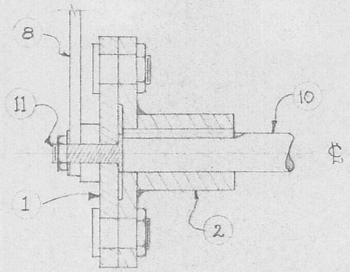

DETAIL OF ECCENTRIC

BILL OF MATERIAL

No.	PART	QUAN.	REFERENCE
1	ECCENTRIC PLATE	1	MK "A"
2	ECCENTRIC HUB	1	"B"
3	TORSION BLOCK	1	"C"
4	BEARING	2	"D"
5	BEARING	2	"E"
6	TORSION ARM	1	"F"
7	TEST BAR		"G"
8	LINK	1	"H"
9	3/4 HP MOTOR	1	
10	1"ϕ x 18" SHAFT	1	
11	½"ϕ BOLT	1	
12			

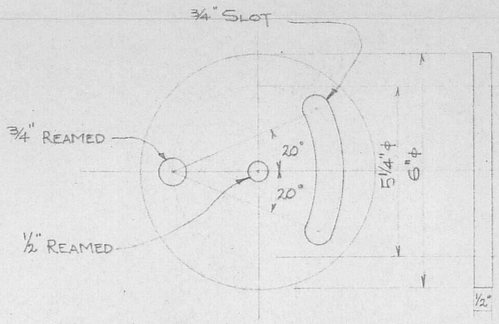

① 1-M·S· ECCENTRIC PLATE MK "A"

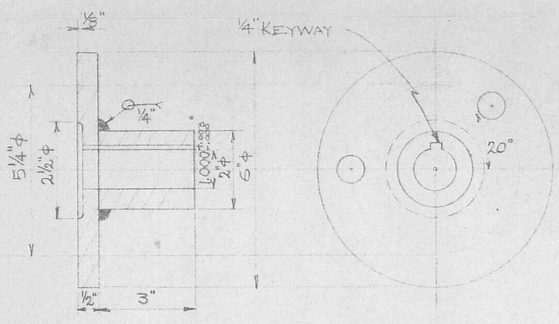

② 1-M·S· ECCENTRIC HUB MK "B"

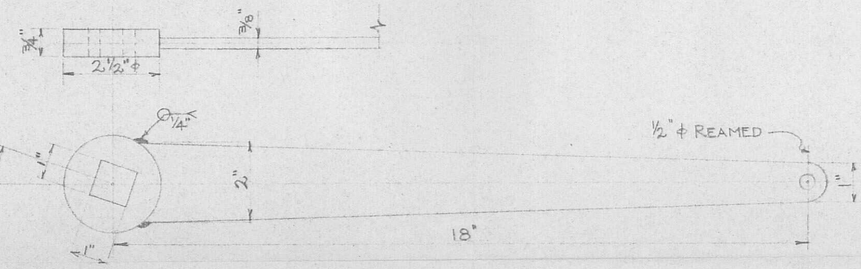

⑥ 1-M·S· TORSION ARM MK "F"

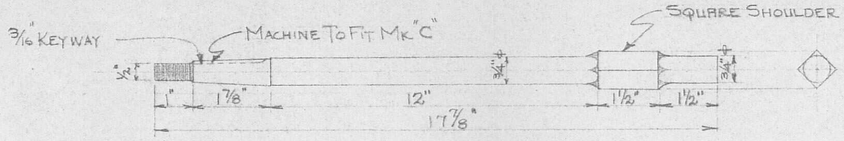

⑦ 1-M·S· TEST BAR MK "G"

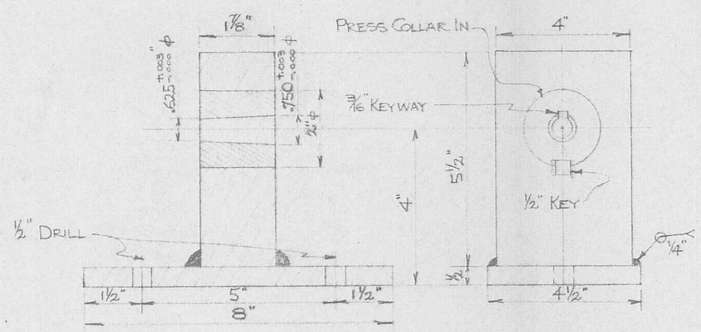

③ 1-M·S· TORSION BLOCK MK "C"

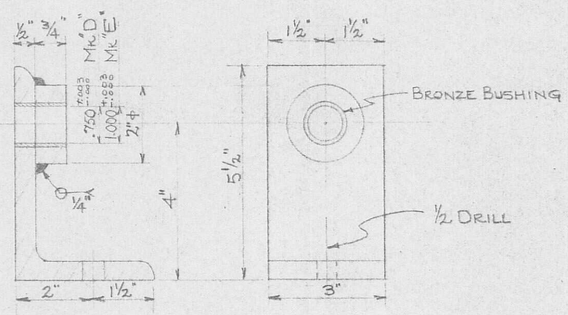

④ 1-M·S· BEARING MK "D"

⑤ 1-M·S· BEARING MK "E"

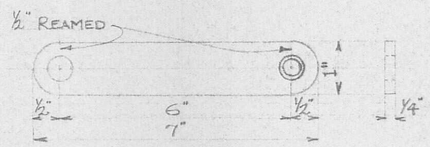

⑧ 1-M·S· LINK MK "H"

MECHANICAL ENGINEERING
UNIVERSITY OF BRITISH COLUMBIA

REVERSED TORSION MACHINE

SCALE	4½"=1'-0"	MAY 1949
DRAWN BY	Wm. C. Leith	DRAWING NO. FIG. 22

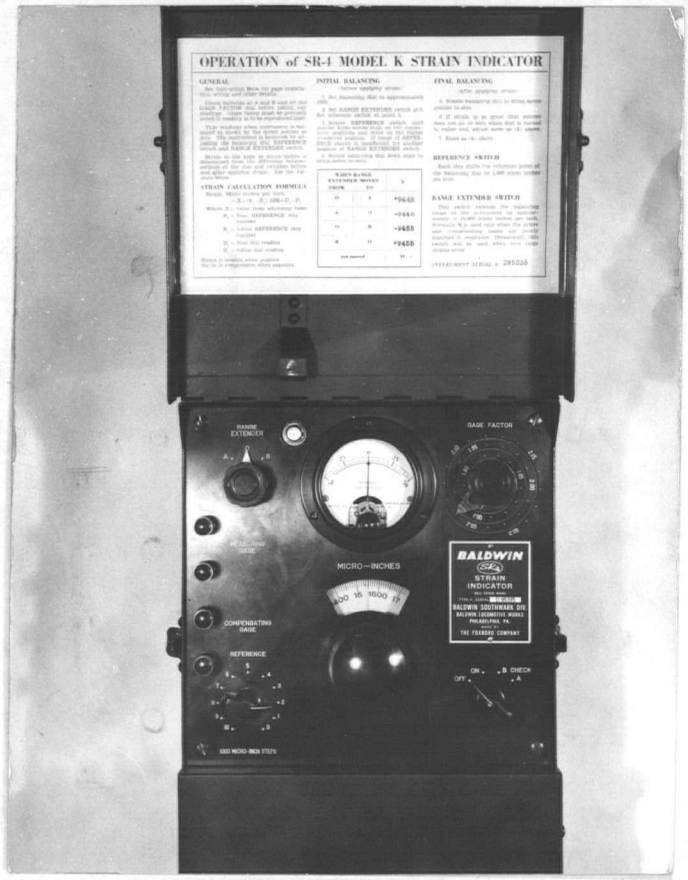

Fig. 23 SR-4 Strain Indicator

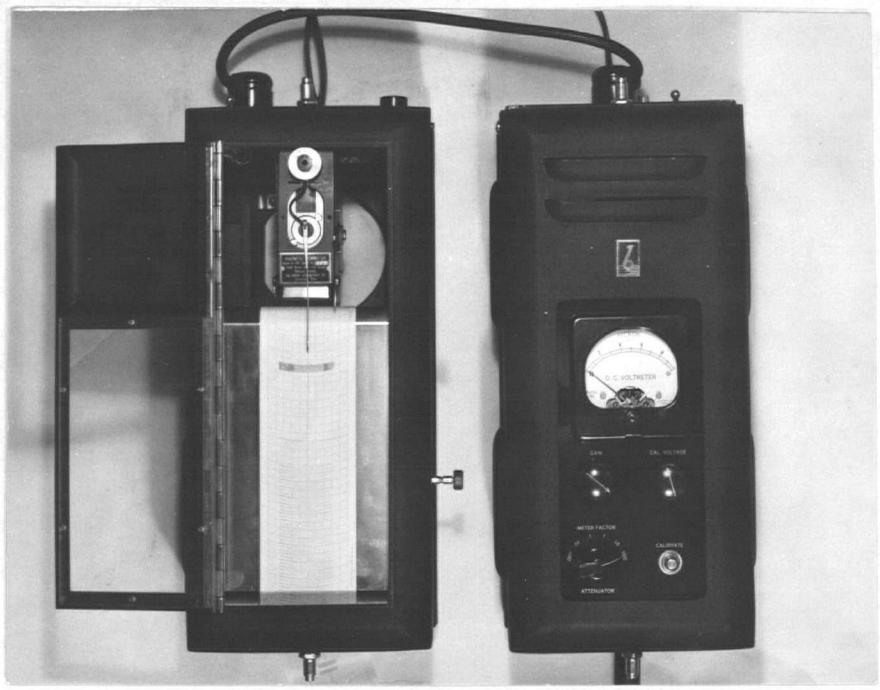

Fig. 24 Brush Oscillograph

The strain and hence the stress in each specimen was calculated from the applied torque which was measured by SR-4 Strain Gages on the torsion arm. These Gages are made of resistance-strain-sensitive wire bonded to a thin paper carrier; they were cemented on the edges of the torsion arm and covered with wax as shown in Fig. 21. When the arm was displaced, one of the Gages was strained in tension and the other in compression. The change in resistance which is proportional to the change in strain, can be measured and converted to stress. Therefore, knowing the strain in the torsion arm, the stress in a specimen could be calculated from the calibration curve shown in Appendix A. The static strains (when the machine was stopped) were measured with the SR-4 Strain Indicator shown in Fig. 23. The dynamic strains (when the machine was running) were measured with the Brush Oscillograph as shown in Fig. 24.

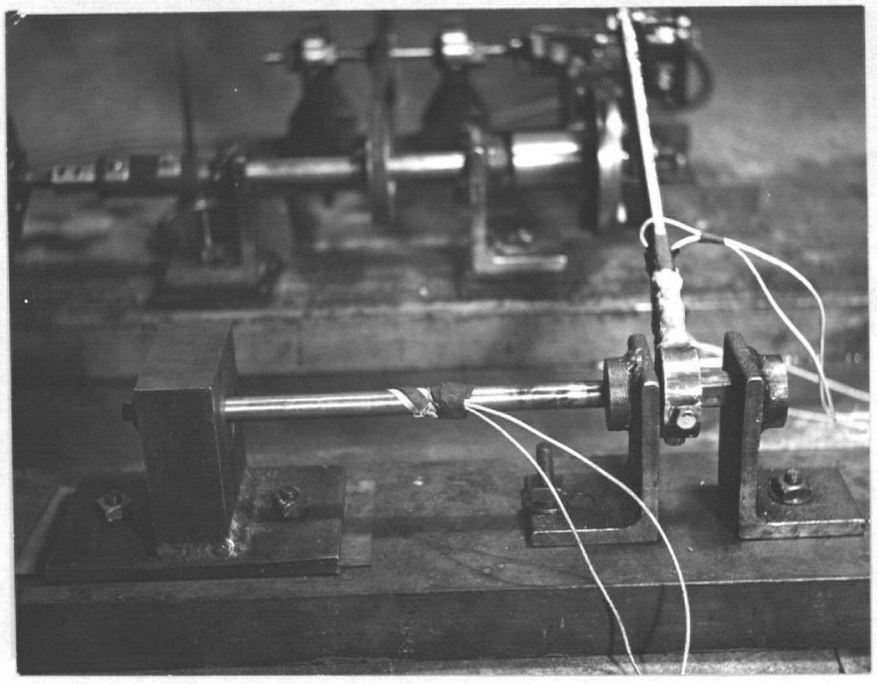

Fig. 25 Location of Strain Gages

Since the static and dynamic stresses agreed within experimental error, the oscillograph curves were used to measure the applied torque. Also, these nominal stresses agreed with the actual stresses in the test shaft measured with a separate strain gage shown in Fig. 25. A complete description of the measuring instruments is given in a paper by Johnson and Bruce (12). The nominal stresses were calculated for each specimen and are shown in Table II.

Combined reversed bending and reversed torsional stresses were imposed on a test shaft when the two bearings supporting the torsion shaft were removed. The torsional stresses were calculated from the applied torque and the bending stresses were measured by strain gages on the test shaft. The nominal stresses were calculated for each specimen and are shown in Table III.

Graphs of the cyclic stresses as measured by the Brush Oscillograph are shown in Fig. 26.

TABLE 11 REVERSED TORSION DATA

Number	Keyway	Torsion Stress	Number of Cycles	Remarks
1	RE	8500	1022200	UMBR
		9400	261700	BR
2	SR	9400	230000	BR at flats
4	SR	8400	275000	BR at fillet
5	RE	8000	312000	BR
6	SR	8000	1163500	BR

SR = sled-runner keyway

RE = round-ended keyway

BR = broken

UNBR = unbroken

$$\text{Torsion Stress} = \frac{Tr}{J}$$

TABLE 111 COMBINED REVERSED BENDING AND TORSION DATA

Number	Keyway	Bending Stress	Torsion Stress	Number of Cycles	Remarks
3	SR	60000	4000	8700	BR
7	RE	3300	9400	14100	BR
8	SR	3300	9400	41000	BR

SR = sled-runner keyway

RE = round-ended keyway

BR = broken

UNBR = unbroken

$$\text{Bending Stress} = \frac{Mc}{I}$$

$$\text{Torsion Stress} = \frac{Tr}{J}$$

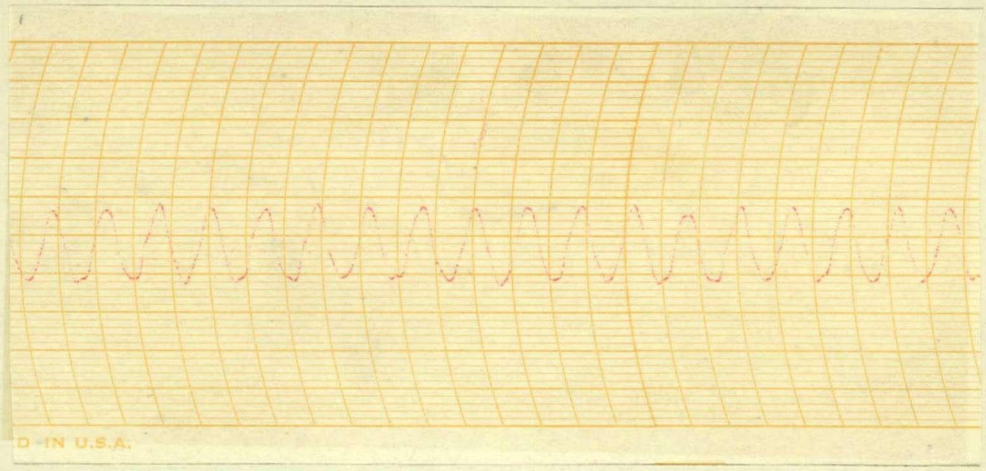

Torsion Test — Torsion Stress

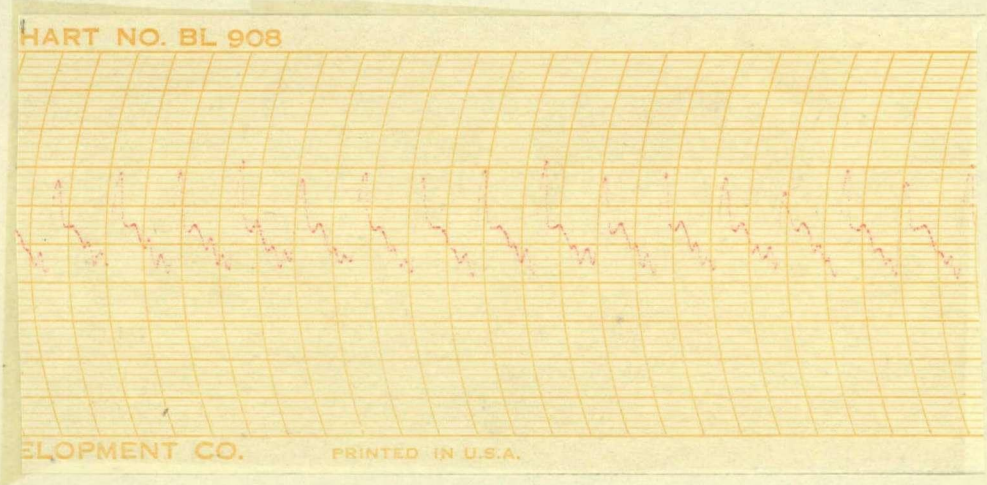

Combined Bending and Torsion Test — Torsion Stress

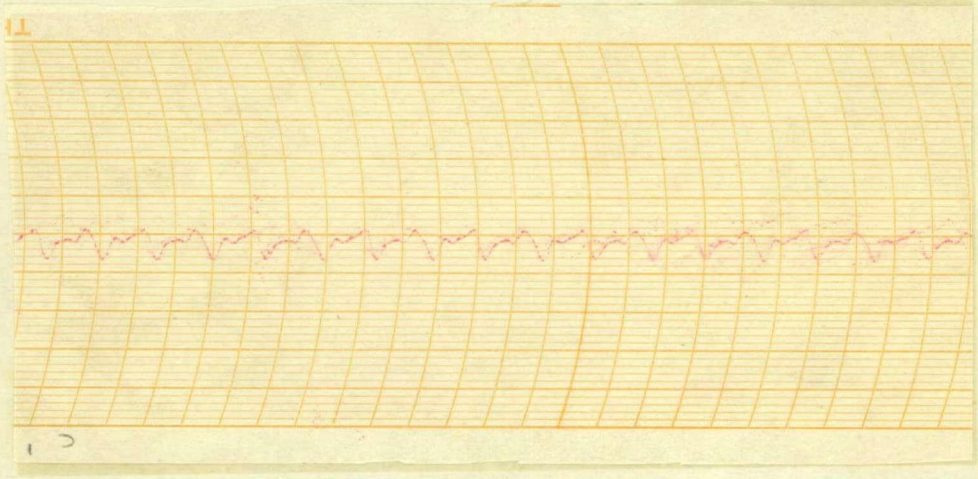

Combined Bending and Torsion Test — Bending Stress

Fig. 26 GRAPHS OF CYCLIC STRESSES

OBSERVATIONS

1. At first the bearings supporting the eccentric shaft heated up and threatened to seize when the maximum eccentricity was applied. On the advice of Professor Wm. Wolfe, Sulfur Flowers was added to the oil. Immediately the bearings cooled to a moderate temperature and the wear from then on seemed negligible. Therefore, Sulfur acts very well as an extreme pressure lubricant, for steel shafts in bronze bushings.

2. All of the shafts tested in the torsion machine, especially ones with sled-runner keyways heated up to a temperature that could hardly be touched. Since this is due to the work done, it may have some effect on the fatigue strength as the shafts were hotter for higher applied stresses.

RESULTS

1. In all cases the sled-runner keyway withstood more cycles at a given stress than the round-ended keyway.

2. Reversed Bending Fractures are shown in Fig. 27.
   (a) the sled-runner keyway showed a circumferential crack on the driving side near the forward end.
   (b) the round-ended keyways broke near the middle of the taper probably resulting from poor fits and a series of power failures.

3. Reversed Torsion Fractures are shown in Fig. 28.
   (a) the sled-runner keyway had a crack start at the root of the forward corners and progressed at 45 degrees to the shaft axis. These cracks became visible at about 500,000 cycles and the writer watched them progress until failure at 1,163,500 cycles. This specimen failed exactly as predicted by the maximum shear theory.
   (b) the round-ended keyway had a radial crack start at each side of the forward end at approximately 45 degrees to the shaft axis.

4. Combined Bending and Torsion fractures are shown in Fig. 29. Both types of keyways had cracks at the forward end and showed some evidence that the angle of fracture is governed by the

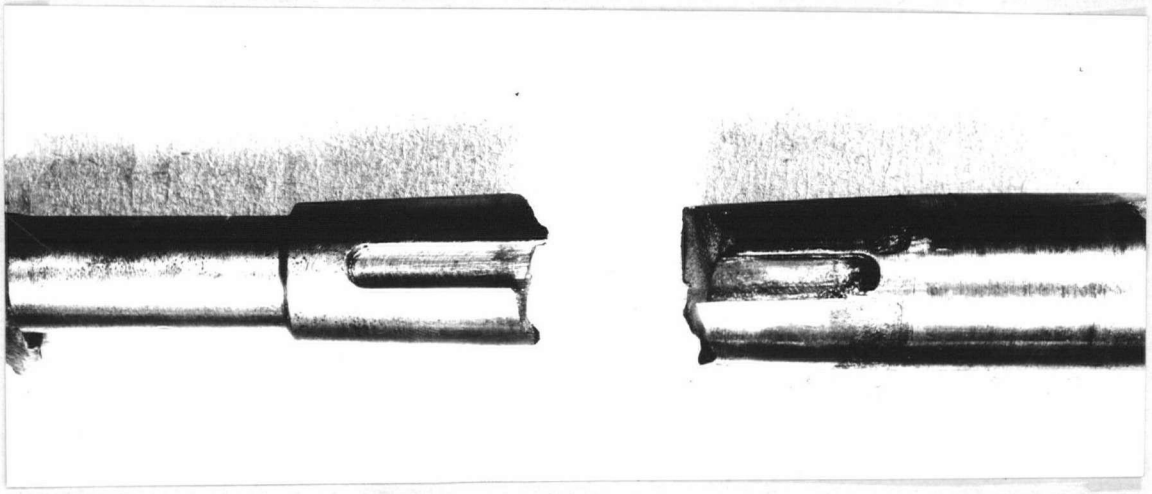

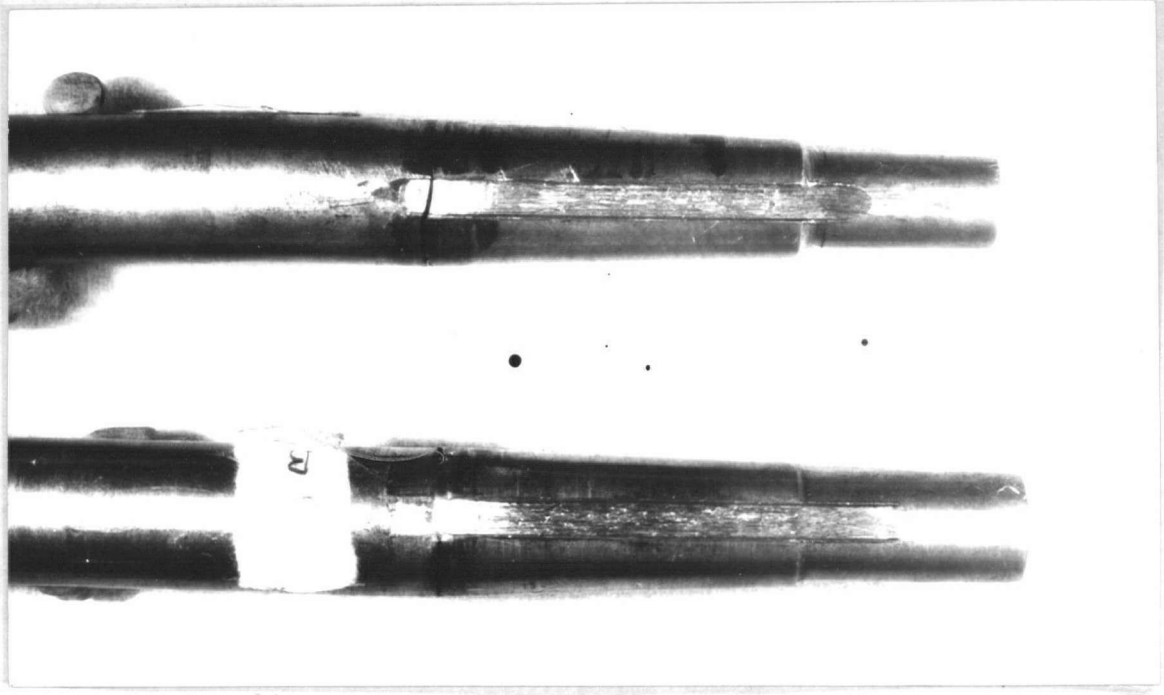

Fig. 26 Reversed Bending Fractures

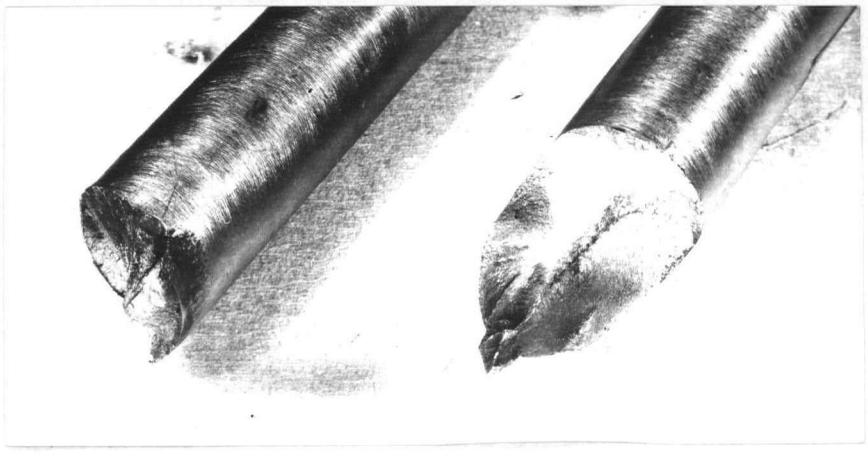

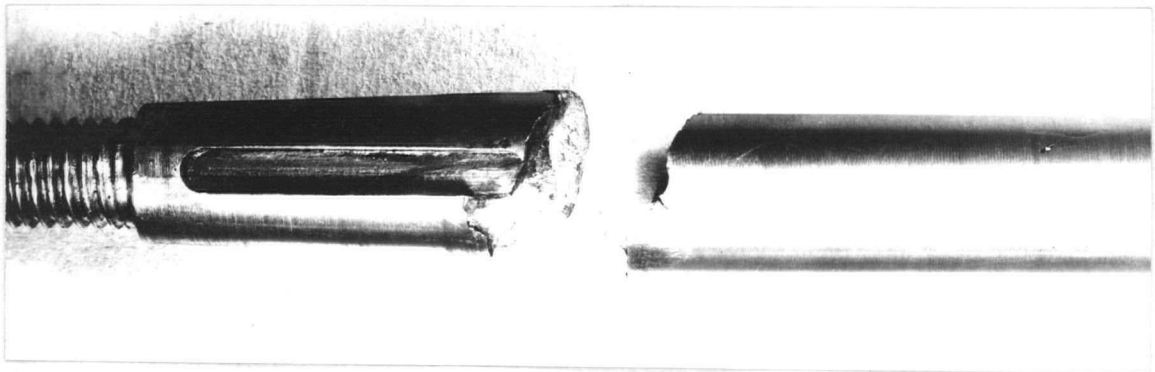

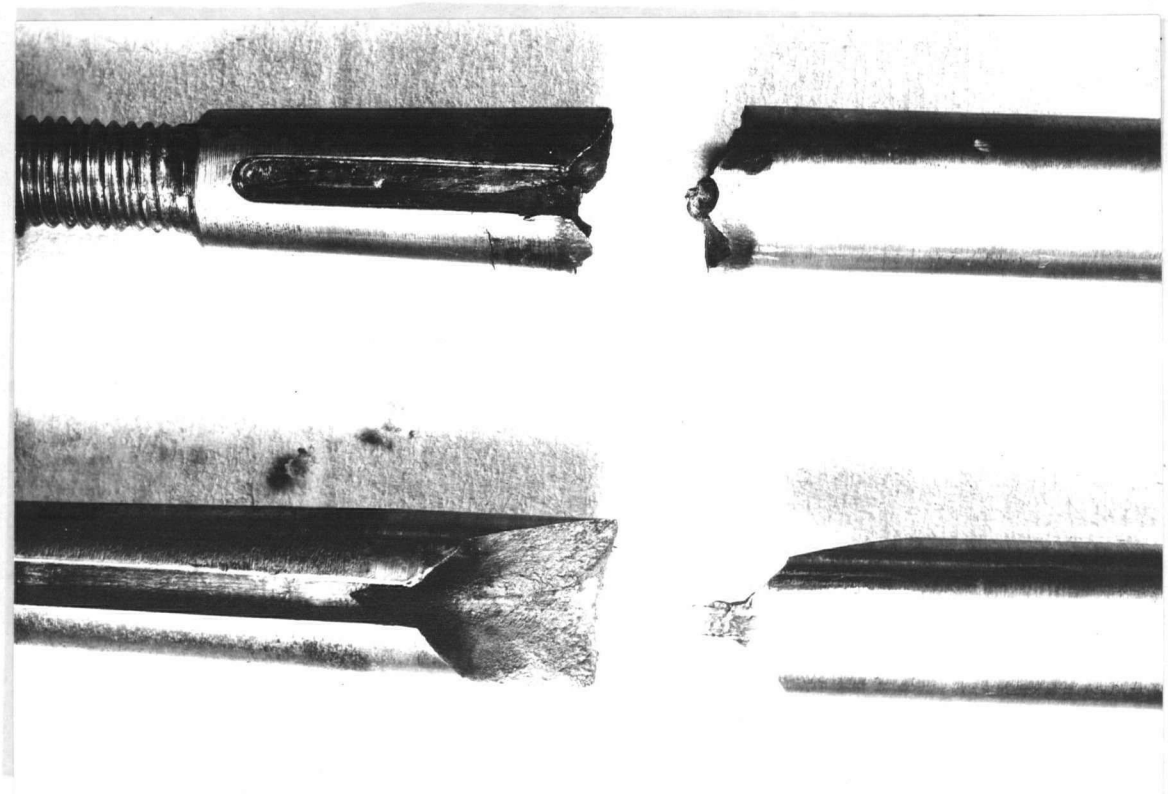

Fig. 27 Reversed Torsion Fractures

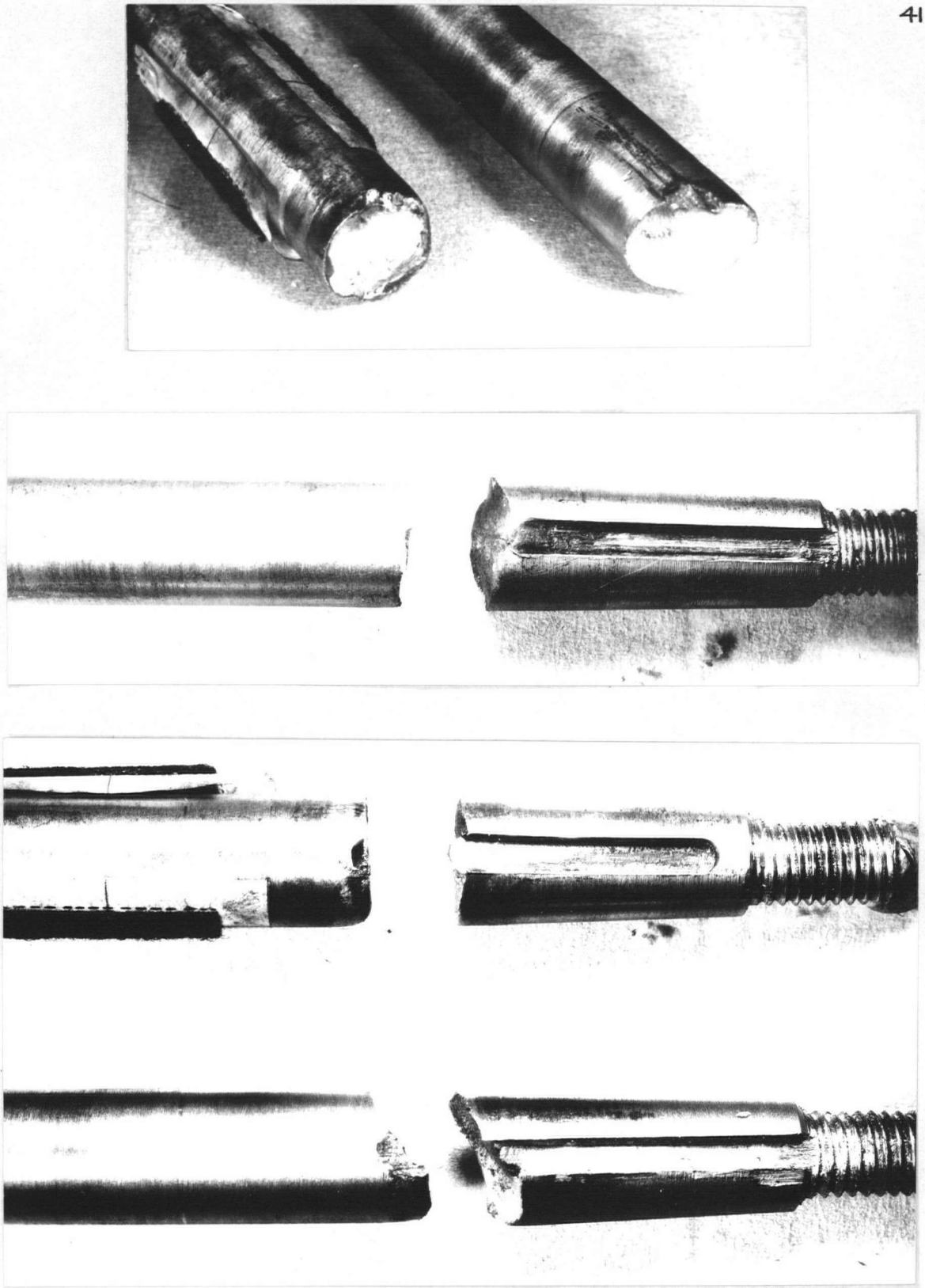

Fig. 28 Combined Reversed Bending and Torsion Fractures

combined stresses.

5. The reversed torsion fracture at a fillet as shown in Fig. 30 had a circumferential crack at the stress raiser with radial cracks pointing towards the centre.

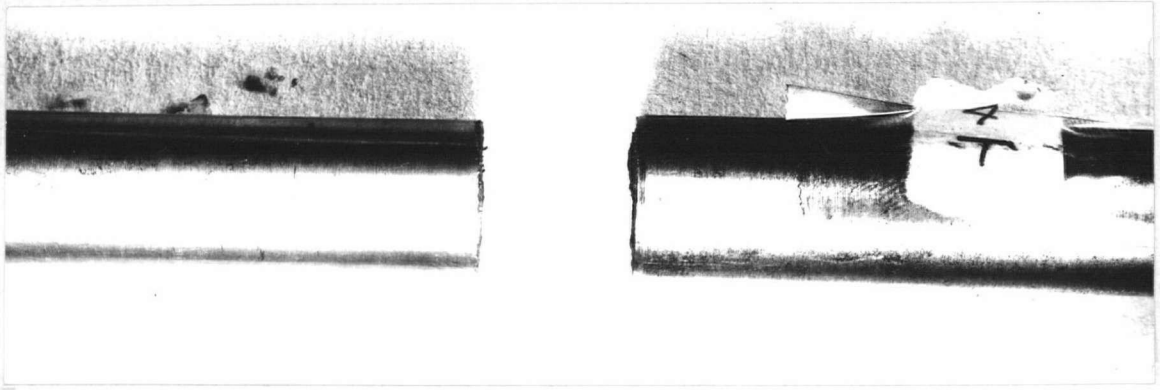

Fig. 30 Reversed Torsion Fracture at a Fillet

6. Sulfur was effectively used as an extreme pressure lubricant for steel on bronze.

CONCLUSIONS

1. A sled-runner keyway has a higher fatigue strength than a round-ended keyway in a keyed tapered-shaft assembly stressed by reversed bending, reversed torsion, or combined reversed bending and reversed torsion.

2. The maximum shear theory of strength predicts the plane of fatigue failure.

   (a) bending stresses produce a circumferential fracture perpindicular to the shaft axis.

   (b) torsional stresses produce a helicoidal fracture at 45 degrees to the shaft axis.

   (c) combined bending and torsional stresses produce a fracture whose angle of inclination to the shaft axis is governed by the combined stress.

3. Owing to size effect, the difference in fatigue strength between the two types of keyways may be less prominent in the actual shaft.

4. The measuring instruments showed that the static and dynamic stresses are equal in the torsion machine.

5. Since little research has been done on the strength of keyed connections, these machines could be useful for further investigations on this subject.

RECOMMENDATIONS

1. Roller bearings would be suitable for the two bearings supporting the eccentric shaft rather than the bronze sleeve.

2. If the torsion arm was reduced to 10 in. of effective length, higher speeds and higher stresses could be used; or for the same conditions, smoother operation would result.

3. For an exact determination of the fatigue strength of keyed connections, the shaft and the bushing should be ground to size. Vancouver Engineering Works has the equipment to do this job.

4. By the use of suitable bushings, both machines could be modified to test straight keyed connections or press fits.

APPENDIX A

The SR-4 Strain Gages which measured the applied torque on the torsion arm were calibrated by static loads using the Baldwin SR-4 Strain Indicator. This indicator consists of a four arm Wheatstone bridge. The strain gages are connected so that the bridge circuit is unbalanced when a change in stress changes the gage resistances.

When a gage is strained in tension its length increases and its diameter decreases with a resultant change in electric resistance. The ratio between the "change in resistance" to the "change in strain" is called the strain sensitivity or the gage factor F. The unit strain is equal to the unit resistance change divided by the gage factor. This indicator reads the strain directly in micro inches.

Fig. 31 shows the calibration curve for the torsion arm to be linear as expected.

CALIBRATION OF TORSION ARM STRAIN GAGES

Fig. 31

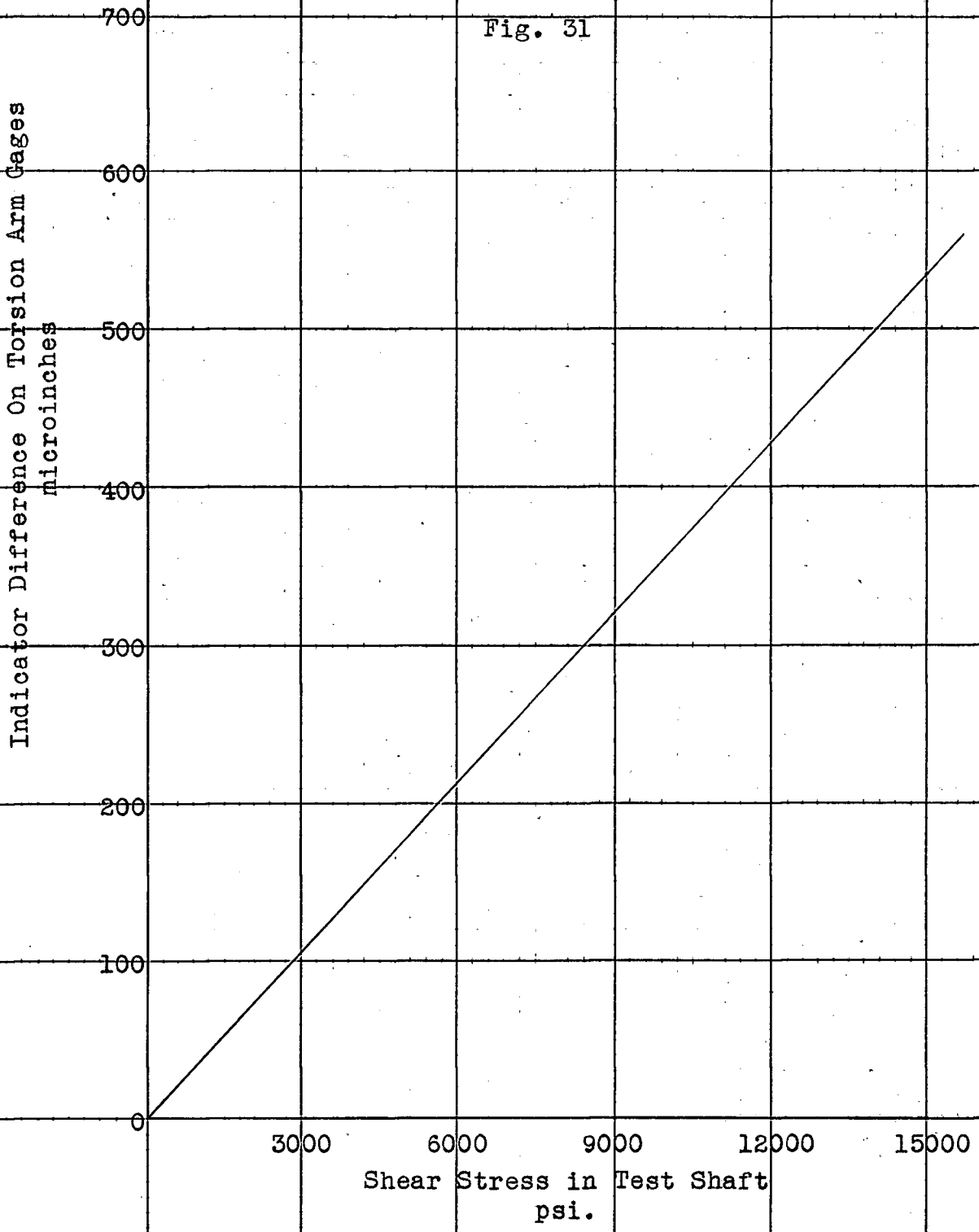

APPENDIX B

To show that the static and dynamic stresses in a torsion test shaft agreed within experimental error. The static strains were measured with the SR-4 Strain Indicator. The dynamic strains were measured with the Brush Oscillograph.

Nominal Stresses

The nominal stresses were calculated for the applied torque measured by the strain gages on the torsion arm as shown in Fig. 25.

(a) Static Load

Maximum Reading = 9920 micro-inches

Minimum Reading = 8920 "

Difference = 1000 "

e = strain = 500 micro-inches

From the calibration curve in Appendix A

$S1 = \pm 13600$ psi.

(b) Dynamic Load

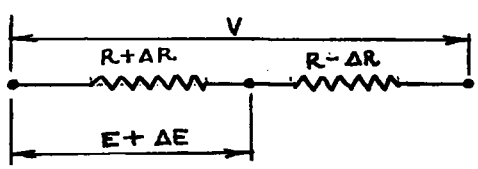

$$I = \frac{V}{2R}$$

$$E+\Delta E = \frac{V}{2R}(R+\Delta R)$$

$$\Delta E = \frac{V}{2}\frac{\Delta R}{R}$$

V = 6 volts

From initial setting

15 mm deflection = 5 milli-volts

7 mm " = 2.33 "

$$\frac{\Delta R}{R} = \frac{2\Delta E}{V} = \frac{2(.00233)}{6} = .0078 \text{ ohms per ohm}$$

$$e = \frac{1}{F}\frac{\Delta R}{R} = \frac{1}{2.06}(.0078) = .000380 \text{ inches}$$

F = gage factor = 2.06

from calibration curve in Appendix A

$S_i = \pm 11000$ psi.

Measured Stresses

The measured stresses were calculated from the strain observed in a strain gage at 45 degrees to shaft axis as shown in Fig. 25.

(a) Static Load

Maximum Reading = 1985 micro-inches

Minimum Reading = 815 "

Difference = 1170 "

$e = 585$ micro-inches

$$e = \frac{1}{E}(S1 + mS2) = \frac{1+m}{E}(S1)$$

$$S_i = \frac{E\,e}{1+m} = \frac{(30 \times 10^6)(585 \times 10^{-6})}{1.3} = \pm 13500 \text{ psi}$$

(b) Dynamic Load

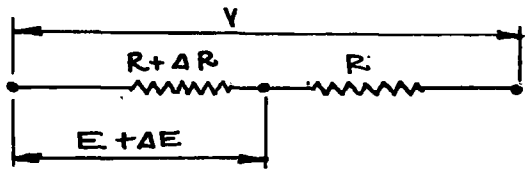

$$E = \frac{V}{2}$$

ΔR = small

V = 6 volts

$$E+\Delta E = \frac{V}{2R+\Delta R}(R+\Delta R)$$

$$\Delta E = \frac{V}{2R+\Delta R}(R+\Delta R) = \frac{V}{2}$$

$$\Delta E = \frac{V}{4}\frac{\Delta R}{R}$$

From initial setting

15 mm deflection = 5 milli-volts

5.5 mm " = 1.83 "

$$\frac{\Delta R}{R} = \frac{4\,\Delta E}{V} = \frac{4(.00183)}{6} = .00122 \text{ ohms per ohm}$$

$$e = \frac{1}{F}\frac{\Delta R}{R} = \frac{1}{2.06}(.00122) = .000590 \text{ inches}$$

$$S_1 = \frac{E\,e}{1+m} = \frac{(30 \times 10^{6})(590 \times 10^{-6})}{1.3} = \pm 13600 \text{ psi}$$

The wire from the strain gages on the torsion arm had to be changed twice because several of the strands broke from the vibration. A broken strand was usually indicated by an unsteady balance on the indicator and erratic curves on the oscillograph.

BIBLIOGRAPHY

1. Archer, S., Screwshaft Casualties - The Influence of Torsional Vibration and Propellor Immersion, London, The Institute of Naval Architects and Marine Engineers, April 8, 1949.

2. Seitz, Fredrick, The Physics of Metals, New York, McGraw Hill Book Co., 1943.

3. Mott, N. F., Atomic Physics and the Strength of Metals, London, The Institute of Metals, Vol.72, Part 6, 1946.

4. Boas, W., Physics of Metals and Alloys, New York, John Wiley and Sons, 1947.

5. Timoshenko, S., Strength of Materials, New York, D. Van Nostrand Co., 2 vols, 1947.

6. Nadai, A., Plasticity, New York, McGraw Hill Book Co., 1931.

7. Solakin, and Karelitz, "Photoelastic Study of Shearing Stresses in Keys and Keyways", ASME, 1931.

8. Frocht, M. M., Photoelasticity, New York, John Wiley & Sons, 2 vols, 1941.

9. Shaw, F. S., "Determination of Stress Concentration Factors," A Symposium of the Fatigue of Metals, Melbourne, University of Melbourne, 1947.

10. Moore, H. F., and Krouse, G. N., Repeated-Stress (Fatigue) Testing Machines Used in the Materials Testing Laboratory of the University of Illinois, Urbana, Ill. Exp. Sta., Circular 23, 1934.

11. Holley, E. G., The Static and Fatigue Torsional Strengths of Various Steels With Circular, Square, and Rectangular Sections, London, The Institute of Mechanical Engineers, September 1940.

12. Johnson, W. J., and Bruce, H. C., Cyclic Stresses in Marine Propellor Shafting, Vancouver, B. C., 1949.

13. Richmond, W. O., Failure of Tail Shafts of Victory Type Steam Cargo Ships, Vancouver, B. C., May 23, 1947.

14. Peterson, R. E., Failure of Shafts Having Keyways, ASTM, 1932.

15. Moore, H. F., The Effect of Keyways on the Strength of Shafts Ill. Exp. Sta., Urbana, Bulletin 42.

16. Dorey, S. F., Limits of Torsional Stress in Marine Oil Engine Shafting, London, The Engineer, April 11, 1947.

17. Gough, H. J., The Fatigue of Metals, New York, D. Van Nostrand Co. Ltd., 1926.

18. Battelle Memorial Institute, Prevention of Fatigue in Metals, New York, John Wiley & Sons, 1946.

19. Richmond, W. O., Progress Report on Research Project - Cyclic Stresses in Ship Propellor Shafting, Vancouver, B. C., February 12, 1949.